Turkish Computational and Theoretical Chemistry

Turkish Comp Theo Chem (TC&TC)

Volume(Issue): 9(3) – Year: 2025 – Pages: 1-24

e-ISSN: 2602-3237

https://doi.org/10.33435/tcandtc.1531766

Received: 12.08.2024 ***Accepted***: 05.09.2024 *Research Article*

Design and Discovery of Lophine Derivatives as Multi-Targeting Agents by Molecular Docking, ADMET, MD Simulation and Pharmacophore Analysis: A Computational Approach

Pujan Sasmal[a,b,1], Shyamal Kumar Biswas[a], Akash Koley[c], Rimpa Jana[a,d], Jagrity Biswas[e]

[a]Department of Pharmaceutical Chemistry, Calcutta Institute of Pharmaceutical Technology & Allied Health Sciences (CIPT & AHS), Uluberia, Howrah, West Bengal - 711 316, India
[b]Department of Pharmaceutical Chemistry, Acharya & BM Reddy College of Pharmacy (ABMRCP), Bengaluru, Karnataka - 560 107, India
[c]Department of Pharmacology, Calcutta Institute of Pharmaceutical Technology & Allied Health Sciences (CIPT & AHS), Uluberia, Howrah, West Bengal - 711 316, India
[d]Department of Pharmaceutical Chemistry, Flemming College of Pharmacy, Baruipur, Kolkata, West Bengal - 700 144, India
[e]School of Health Sciences, The Neotia University, Diamond Harbour Road, South 24 Parganas, West Bengal - 743 368, India

Abstract: Lophine is one of the new core moieties with substitution of three phenyl rings at 2nd, 4th, and 5th position of the imidazole. Lophine is not explored in development of drug molecules. In this research, we have designed 30 lophine derivatives with different substituted functional groups. The designed compounds were evaluated through different in-silico tools and softwares to check their properties for different biological receptors. Molecular docking study was carried out on different receptors i.e. EGFR for anti-cancer, COX-1, and COX-2 for anti-inflammatory, fungal oxidoreductase for anti-fungal, bacterial DNA gyrase for anti-bacterial and TNF-α, which co-relates different type of inflammatory diseases. The molecular docking results revealed that the SAP-28 has significant binding energies -9.8, -9.6 and -10.0 kcal/mol against EGFR, fungal oxidoreductase, and TNF-α receptors respectively. SAP-26 has potent interaction -9.8 and -11.0 kcal/mol against EGFR and COX-2 receptors respectively. Whereas, SAP-25 and SAP-19 showed the best interaction for bacterial DNA gyrase (-8.9 kcal/mol) and COX-1 receptor (-9.7 kcal/mol) respectively. To enhance the acceptability top docked compounds, the ADME parameters along with toxicity analysis were carried out where all the compounds showed acceptable results. Furthermore, the stability of the protein-ligand complexes were determined by a 100 ns MD simulation analysis. The common pharmacophore was generated with the help of the top compounds in the PharmaGist web server.

Keywords: Lophine, molecular docking, ADME, toxicity, MD simulation, pharmacophore, multi-target.

1. Introduction

The derivatives of imidazole, an aromatic heterocyclic compound under the diazole class which has two heteroatoms (nitrogen), have shown high efficacy in many diseases [1,2]. Although the imidazole scaffold may be found in many natural compounds, most imidazoles employed in medicine today are synthetic molecules. These five-membered heteroaromatic compounds have been utilized as anticancer (dacarbazine, zoledronicacid, azathioprine, and tipifarnib) [3], antifungal (clotrimazole, miconazole, ketoconazole, and oxiconazole) [4], antibiotic (Bacitracin) [5], antiparasitic (metronidazole, benznidazole, ornidazole, and secnidazole) [6], antihistaminic (cimetidine, imetit, immepip, and thioperamide) [7,8], antihypertensive (losartan, eprosartan, and olmesartan) [9–11], and anti-inflammatory (celecoxib) [12–14] medicines since their discovery in the early 1840s [15]. Since 1877 there are 36

[1] Corresponding Authors
e-mail: pujansasmal@gmail.com

crystal structures of lophine (2,4,5-triphenyl-1H-imidazole). With the dihedral angles of 21.4˚, 24.7˚, and 39.0˚ the three phenyl rings attach in the 2, 4, and 5 positions of the imidazole ring respectively in a non-coplanar manner [16,17]. Due to its bright yellow hue when it interacts with oxygen in the presence of a strong base, it has been used as a chemiluminescent agent by scientists since its discovery [18,19]. In 2013, da Costa et al. produced tacrine-lophine hybrids through a one-pot, four-component synthesis and reported its activity as acetyl- and butyrylcholinesterase inhibitors, paving the way for the lophine derivative to be used as a physiologically active molecule [20]. Recently Lopes et al. has reported new lophine-carbohydrate hybrids containing cholinesterase inhibitor property [21].

Inflammation functions as a protective mechanism for wounded tissues, shielding them from diverse stimuli and facilitating their recovery while eradicating destructive agents [22]. Vasodilation is one of the parallel processes that occur concurrently with inflammation, in which leukocytes migrate from blood vessels to the injury site and cytokines are produced [23,24]. Comparatively to other small molecules, imidazole is a potent inhibitor of multiple inflammatory parameters, including cyclooxygenase 1 (COX-1), cyclooxygenase 2 (COX-2), microsomal prostaglandin E2 synthase (mPGES-1), cytosolic phospholipase A2α (cPLA2α), phosphodiesterase 4 (PDE4), and lipoxygenase (LOX), and also upon nuclear factor κ B (NF-κB) and p38 mitogen-activated protein kinase (p38 MAPK) [15]. Recently Nascimento MVPS et al. reported that tetra-substitute imidazole-containing compounds can inhibit nitric oxide metabolites and pro-inflammatory cytokine (TNF-α, IL-6, and IL-1β) secretion in J774 macrophages which was stimulated with LPS (lipopolysaccharide) [25]. Among the reported compounds "methyl 1-allyl-2-(4-fluorophenyl)-5-phenyl-1H-imidazole-4-acetate" showed the best potency [25].

Cancer is the uncontrolled proliferation of cells that may invade or spread to other parts of the body [26]. RTKs are cell surface receptors that possess a high affinity for polypeptide growth factors, cytokines, and hormones. Most of the biological functions such as cell proliferation, differentiation, survival, metabolism, migration, and cell cycle control are all regulated by receptor tyrosine kinases [27,28]. The epidermal growth factor receptor (EGFR) or HER-1 is one of the four members of the tyrosine kinase family along with ErbB2/HER-2, ErbB3/HER-3 and ErbB4/HER-4 receptor [29–31]. EGFR is activated through ligand-dependent and ligand-independent pathways, as well as by receptor upregulation (a situation noted commonly in cancer) [32,33]. The EGFR expression is associated with the RAS/RAF/mitogen-activated protein kinase pathway [30], Phosphatidylinositol 3-kinase/Akt pathway, Phospholipase Cγ activation [30], Signal transducers and activators of transcription pathway, Src kinase pathway [30], Endocytotic pathway [34], Stress pathway [34], Autophagy pathway [34]. The upregulation of EGFR has been associated with increased aggressiveness and poor clinical outcomes in a variety of cancer tissues, including breast, lung, ovarian, cervical, bladder, oesophageal, brain, and head and neck cancers [35]. Heppner DE et al. in the year 2020 reported the tetrasubstituted imidazole molecules as the potent inhibitors of the EGFR receptor [36]. They also reported the binding nodes of the tetrasubstituted imidazole against mutant EGFR: EGFR(T790M/V948R), EGFR(L858R/T790M), EGFR(L858R/T790M), EGFR(L858R/T790M/C797S), EGFR(L858R/T790M/C797S).

Tumour necrosis factor-alpha (TNF-α), an inflammatory cytokine generated by macrophages/monocytes during acute inflammation, causes a variety of cell signalling pathways that cause necrosis or apoptosis. TNF-α is mostly produced by immune cells in response to pathogen- or danger-associated molecular patterns (PAMPs or DAMPs), although it may also be produced by endothelial cells, microglia, cardiac myocytes, and fibroblasts [37]. TNF-α stimulates proliferation and cellular differentiation at the cellular level, as well as inducing proinflammatory gene expression patterns [38,39].

The earliest class of synthetic antifungal drugs are azole chemicals such as imidazoles and triazoles [40,41]. It's widely assumed that the imidazole ring can effectively combine with the iron(II) ion of heme to prevent fungus growth by blocking ergosterol biosynthesis [15]. One of the most notable medical advances in the last century has been the creation of antibacterial medicines to treat

infections [42,43]. The potent effects of imidazole-containing drugs made them very popular in antibacterial treatments. The growing resistance of microorganisms to antibiotics has become a severe issue in recent years. In epidemiology, multidrug-resistant bacteria such as Escherichia coli, Klebsiella pneumoniae, Acinetobacter baumanii, etc. are the most important [44]. The prevalence of antimicrobial resistance in both human and animal diseases is rising.

Very few lophine derivatives have been identified as bioactive molecules. In this study, we developed various lophine derivatives and examined them computationally against five distinct receptors, including COX for inflammatory, EGFR for cancer, TNF- α, bacterial DNA gyrase, and fungal oxidoreductase, using molecular docking and other techniques. In addition, ADME investigations, toxicological parameters, and target prediction were conducted. To determine the stability of the protein-ligand complexes, 100 ns of MD simulation tests were performed. The common pharmacophore was then constructed for the compounds with the highest hit rate.

2. Computational Methods

2.1. Molecular design

Lophine is tri-substituted imidazole derivative at 2nd, 4th and 5th position. Through the extensive literature survey, 30 lophine derivatives were designed computationally [45]. The phenyl rings of the compound make it easier to introduce any pharmacophoric functional group as per the receptor cavity and make it more favorable for a multi-targeting moiety.

2.2. Molecular docking studies

The Molecular docking study is one of the important computational approach to determine the "Best-Fit" interaction between ligand and receptor [46]. This method is widely used for lead optimization in the process of drug discovery and development. The molecular docking was carried out in AutoDock Vina v.1.2.0 on DELL system with Windows 10, 64-bit OS, 8 GB RAM, and an Intel(R) Core(TM) i5-7200U CPU with 2.5 GHz processor [47].

2.2.1. Selection of proteins

Molecular docking was performed representative proteins of different diseases in this research. EGFR protein with PDB ID: 5HG7 [48] and1.85 Å resolution was considered for the docking studies. For the docking studies of COX-1, PDB 3KK6 [49] was considered (co-crystallized with celecoxib and with a resolution of 2.75 Å). The PDB 3LN1 [50] was considered for the COX-2 protein which is co-crystallized with celecoxib and with a resolution of 2.40 Å. To evaluate the anti-fungal activity the PDB 1AI9 [51] which is the oxidoreductase enzyme of Candida albicans with a resolution of 1.85 Å was considered. DNA gyrase enzyme with the PDB ID: 5L3J [52] with the resolution of 2.83 was considered for the evaluation of antibacterial activity through the In-silico pathway. Finally, the activity against the TNF-α was evaluated by taking the PDB 6OP0 [53] with a resolution of 2.55 Å.

2.2.2. Protein preparation

The PDB files of all the proteins were retrieved from Research Collaboratory for Structural Bioinformatics (RCSB) Protein Data Bank (https://www.rcsb.org/) [54]. The water molecules, as well as the unwanted amino-acid chains, were removed by using the Biovia Discovery Studio Visualizer [55]. The energy minimization of the protein was carried out on the Swiss-PdbViewer v4.1 by using the Steepest Descent method of energy minimization [56]. The Kollman charge was added followed by the addition of all polar hydrogen atoms with the help of AutoDock Tools [57]. The grid boxes were generated by taking the grid dimensions of 24*24*24 Å at a grid resolution of 1 Å and the grid box resolution was set according to the position of the crucial amino acids, interacted by the co-crystal ligands. The dimensions were set as grid center: x = -7.099, y = 18.955, z = -26.219 for EGFR protein, x = -33.649, y = 43.259, z = -4.846 for COX-1 protein, x = 30.274, y = -24.206, z = -15.586 for COX-2 protein, x = 28.932, y = -5.96, z = 14.441 for the oxidoreductase enzyme of Candida albicans, x = -13.007, y = 12.783, z = 18.168 for DNA Gyrase enzyme of bacteria and x = -11.084, y = -1.565, z = 17.475 for the TNF-α receptor.

2.2.3. Ligand Preparation

All the substituted lophine or substituted triphenyl imidazole moiety was designed and sketched for this In-silico by using the ChemSketch Freeware application. The ligand PDB file (.pdb) was prepared with the help of the PRODRG web server (http://davapc1.bioch.dundee.ac.uk/cgi-bin/prodrg)

by using the topology of the structure files and adding the polar hydrogens [58]. Finally, the PDBQT (.pdbqt) files were generated by adding the gasteiger charge and assigning atoms to the AutoDock-4 (AD4) type with the help of AutoDock Tools software.

2.2.4. Docking

The molecular docking was executed by using the AutoDock Vina script [47]. Nilotinib [59], Celecoxib [60], Itraconazole [61], Metronidazole [62], A7A Ligand (co-crystal ligand of TNF-α with PDB ID: 6OP0) [53] were considered for the standard molecules of EGFR, COX-1 and COX-2, anti-fungal, antibacterial and TNF-α inhibitor activity. The Local Gradient Optimization approach was used as a scoring function to find the optimal binding postures for the developed lophine molecules and various proteins. The binding energy (kcal/mol) and the number of binding interactions were used to analyze the molecular docking results. The protein-ligand complex was analysed by the BIOVIA discovery studio visualizer 2021 [55].

2.2.5. Validation of molecular docking

The validation of the molecular docking protocol was accomplished by removing the co-crystal ligands from the binding pocket and re-docked the same in the same binding pocket and evaluating the Root-Mean-Square Deviation (RMSD) after superimposing both the protein-ligand complexes.

2.3. Drug-likeness study and molecular properties

In this current study, the drug-likeness parameters of the compounds were evaluated based on Lipinski's Rule of Five and Veber's Rule [63,64]. The top 7 compounds with the highest docking score (in terms of binding energy) were considered for the drug-likeness properties. Different parameters like molecular weight, the number of hydrogen bond donors/acceptors, polar surface area, the number of rotatable bonds, partition coefficient, etc. were determined. SwissADME web server (http://www.swissadme.ch/) was utilized to predict the Absorption, Distribution, Metabolism and Excretion (ADME) of the molecules [65]. The Simplified Molecular Input Line Entry System (SMILES) format of the molecules was uploaded to the SwissADME web server and the results were downloaded and analyzed manually. The Brain Or IntestinaL EstimateD permeation method (BOILED-Egg) was used to determine the pharmacokinetics and bioavailability of the compounds [66].

2.4. Toxicity studies

The toxicological parameters of the top 7 docked molecules were examined at the mcule toxicity checker web server (https://mcule.com/apps/toxicity-checker/). This web server provides the toxicological parameters in terms of yes or no. The detailed toxicological studies were verified in the ProTox-II web server (https://tox-new.charite.de/protox_II/) [67]. Here different toxicological parameters like Hepatotoxicity, Carcinogenicity, Immunotoxicity, Mutagenicity, LD50, etc. of the compounds were inspected.

2.5. Biological activity predictions of the compounds

Kinase inhibitors are those molecules that target protein kinases that have been changed in cancer cells and are thought to be responsible for part of the cancer cells' uncontrolled development. The In-silico kinase inhibitor activity prediction of the best molecules was carried out on the Molinspiration Cheminformatics Software web server (https://www.molinspiration.com/) to re-verify the kinase inhibition. The SMILES format of all the compounds was submitted to the webserver and the results were retrieved. Moreover, the designed top molecules may possess some other biological activity along with the chosen disease. Thus, the detailed target prediction of the top small molecules was examined in the SwissTargetPrediction web server (http://www.swisstargetprediction.ch/) [68]. Here based on the molecular structure and functional groups present in the molecules, the probable biological targets can be predicted along with the percentage of biological activity.

2.6. Molecular dynamics (MD) simulation

MD studies were performed using the software named 'WebGRO for Macromolecular Simulations' (https://simlab.uams.edu/index.php) by the University of Arkansas for Medical Sciences, Little Rock, US. It utilizes GROMACS (GROningen MAchine for Chemical Simulations) [69] software for performing MD simulations. Here, the docked protein-ligand complex was

extracted and the ligand coordinates were inserted into the PRODRG webserver [70] to get the ligand topology files. The ZIP file from the PRODRG web server as well as the PDB file of the docked protein-ligand complex was uploaded to the WebGRO server. GROMOS96 43a1 force-field was used to minimize the energy in the 'steepest descent' method at 5000 steps run and 100 nanosecond run time at T = 310K, constant volume 'V', constant number of atom = N (NVT); and constant pressure P = 1.0bar (NPT). Leap-frog MD integrator was used and 1000 was marked as the approximate number of frames per simulation. Simple Point-Charge (SPC) water model was utilized in a triclinic grid box and nutrilized by 0.15 M NaCl salt. MD trajectories were analyzed for Root-mean-square deviation (RMSD) of protein and ligand, Root-mean-square fluctuations (RMSF), the radius of gyration (Rg), and protein-ligand hydrogen bonding during the 100 nanoseconds MD runtime.

2.7. Common pharmacophore generation

Finally, the common pharmacophore of the top docked molecules was generated with the help of PharmaGist web server (https://bioinfo3d.cs.tau.ac.il/PharmaGist/php.php) [71]. The top docked ligands were converted to Sybyl mol2 format with the help of Open Babel software v2.4.0. The ".zip" extension of the top ligands was uploaded to the PharmaGist webserver. The output results were analyzed in BIOVIA Discovery Studio Visualizer 2021.

3. Results and discussion

3.1. Molecular design and strategic applications

Based on the literature surveys and randomized substitution, the molecular design was performed. A total of 30 substituted lophine or substituted triphenyl imidazole were designed (Table 1). Different substitutions were implemented to the phenyl ring, present in the 2nd position of the imidazole.

Table 1. Molecular Design of the lophine molecules

Compound Code	IUPAC Name	Substitution Implemented
SAP-1	2,4,5-triphenyl-1H-imidazole	---
SAP-2	2-(4-nitrophenyl)-4,5-diphenyl-1H-imidazole	4-nitro
SAP-3	2-(3-nitrophenyl)-4,5-diphenyl-1H-imidazole	3-nitro
SAP-4	2-(2-nitrophenyl)-4,5-diphenyl-1H-imidazole	2-nitro
SAP-5	2-(2,4-dinitrophenyl)-4,5-diphenyl-1H-imidazole	2,4-dintro
SAP-6	2-(3-bromophenyl)-4,5-diphenyl-1H-imidazole	3-bromo
SAP-7	2-(4-bromophenyl)-4,5-diphenyl-1H-imidazole	4-bromo
SAP-8	2-(4-chlorophenyl)-4,5-diphenyl-1H-imidazole	4-chloro
SAP-9	2-(2-chlorophenyl)-4,5-diphenyl-1H-imidazole	2-chloro
SAP-10	2-(3-chlorophenyl)-4,5-diphenyl-1H-imidazole	3-chloro
SAP-11	2-(2,4-dichlorophenyl)-4,5-diphenyl-1H-imidazole	2,4-dichloro
SAP-12	2-(3,4-dichlorophenyl)-4,5-diphenyl-1H-imidazole	3,4-dichloro
SAP-13	2-(2,6-difluorophenyl)-4,5-diphenyl-1H-imidazole	2,2-difluoro
SAP-14	2-(3,4-dimethoxyphenyl)-4,5-diphenyl-1H-imidazole	3,4-dimethoxy
SAP-15	4-(4,5-diphenyl-1H-imidazol-2-yl)benzene-1,2-diol	3,4-dihydroxy
SAP-16	4-(4,5-diphenyl-1H-imidazol-2-yl)-N,N-dimethylaniline	4-(N,N-dimethyl)amino
SAP-17	2-(4-ethoxyphenyl)-4,5-diphenyl-1H-imidazole	4-ethoxy
SAP-18	2-(4-fluorophenyl)-4,5-diphenyl-1H-imidazole	4-fluoro
SAP-19	2-(4,5-diphenyl-1H-imidazol-2-yl)phenol	2-hydroxy
SAP-20	3-(4,5-diphenyl-1H-imidazol-2-yl)phenol	3-hydroxy
SAP-21	4-(4,5-diphenyl-1H-imidazol-2-yl)phenol	4-hydroxy
SAP-22	5-(4,5-diphenyl-1H-imidazol-2-yl)-2-methoxyphenol	3-hydroxy-4-methoxy
SAP-23	2-(4-methoxyphenyl)-4,5-diphenyl-1H-imidazole	4-methoxy
SAP-24	2-(3-methoxyphenyl)-4,5-diphenyl-1H-imidazole	3-methoxy
SAP-25	4,5-diphenyl-2-(o-tolyl)-1H-imidazole	2-methyl
SAP-26	4,5-diphenyl-2-(m-tolyl)-1H-imidazole	3-methyl

SAP-27	4,5-diphenyl-2-(p-tolyl)-1H-imidazole	4-methyl
SAP-28	4-(4-(4,5-diphenyl-1H-imidazol-2-yl)phenyl)pyridine	4-pyridinyl
SAP-29	5-(4,5-diphenyl-1H-imidazol-2-yl)benzene-1,2,3-triol	3,3,4-trihydroxy
SAP-30	4,5-diphenyl-2-(3,4,5-trimethoxyphenyl)-1H-imidazole	3,3,4-trimethoxy

Table 2. Interaction affinity of substituted lophine molecules

Compound Code	5HG7 (EGFR) (kcal/mol)	3KK6 (COX-1) (kcal/mol)	3LN1 (COX-2) (kcal/mol)	1AI9 (Oxidoreductase) (kcal/mol)	5L3J (DNA Gyrase) (kcal/mol)	6OP0 (TNF-α) (kcal/mol)
SAP-1	-8.7	-9.5	-10.7	-7.2	-7.6	-8.7
SAP-2	-9.4	-7.8	-9.2	-8.3	-7.5	-9.6
SAP-3	-8.5	-7.8	-8.6	-7.5	-7.7	-8.8
SAP-4	-8.8	-7.1	-9.4	-8.6	-8.4	-9.7
SAP-5	-8.9	-7.8	-7.6	-8.2	-8.0	-8.0
SAP-6	-9.5	-9.0	-10.5	-7.4	-8.3	-9.6
SAP-7	-9.4	-9.1	-8.9	-7.3	-7.5	-9.5
SAP-8	-9.4	-8.9	9.8	-8.5	-7.6	-9.6
SAP-9	-8.6	-9.4	-10.5	-7.4	-8.2	-9.6
SAP-10	-9.6	-9.2	-10.7	-7.5	-8.3	-9.7
SAP-11	-8.6	-7.5	-9.9	-7.6	-8.1	-9.4
SAP-12	-9.7	-9.2	-8.3	-8.6	-7.7	-9.9
SAP-13	-9.5	-9.6	-10.8	-8.6	-8.6	-8.6
SAP-14	-8.3	-7.9	-6.6	-7.3	-8.2	-7.2
SAP-15	-9.4	-7.5	-10.7	-7.9	-7.9	-9.7
SAP-16	-9.3	-8.7	-6.2	-8.4	-7.8	-9.2
SAP-17	-7.9	-8.0	-8.7	-7.7	-7.5	-8.8
SAP-18	-9.4	-9.0	-10.8	-7.7	-8.2	-9.4
SAP-19	-9.0	-9.7	-10.3	-7.4	-8.3	-8.3
SAP-20	-9.1	-9.1	-10.2	-7.5	-7.6	-8.6
SAP-21	-9.2	-9.0	-10.4	-8.2	-7.7	-9.1
SAP-22	-9.3	-7.7	-9.3	-8.0	-7.9	-9.6
SAP-23	-9.1	-8.9	-9.7	-7.8	-7.6	-9.2
SAP-24	-9.4	-9.0	-10.5	-7.3	-8.0	-9.6
SAP-25	-9.3	-7.8	-9.6	-8.1	-8.9	-9.4
SAP-26	-9.8	-9.2	-11.0	-7.5	-8.4	-9.8
SAP-27	-8.4	-7.3	-8.8	-7.6	-8.2	-8.7
SAP-28	-9.8	-7.7	-7.0	-9.6	-8.4	-10.0
SAP-29	-9.3	-8.2	-8.4	-7.7	-7.6	-9.3
SAP-30	-7.8	-7.2	-8.1	-7.6	-7.5	-8.2
Standard Compound	-11 (Nilotinib)	-7.4 (Ibuprofen)	-11.1 (Celecoxib)	-10.0 (Itraconazole)	-5.4 (Metronidazole)	-13.7 (A7A Ligand)

3.2. Molecular docking analysis

The molecular docking was performed by using the AutoDock Vina module. The substituted lophine showed a good docking score in terms of interaction affinity. The values of interaction affinities are given in table 2. The compound SAP-19, SAP-25, SAP-26, and SAP-28 shows the best docking score with the selected different receptors. Rather than these the SAP-12, SAP-13 and SAP-18 showed satisfied docking scores. The compound SAP-26 as well as SKB-28 was found to be most active against the EGFR (PDB ID: 5HG7) with the interaction affinity of -9.8 kcal/mol which is near to the standard tyrosine kinase inhibitor drug nilotinib with the interaction affinity of -11.0 kcal/mol. The compound SAP-19 was found to be most active against the COX-1 receptor (PDB ID: 3KK6) with the docking score of -9.7 kcal/mol which is quite higher than the standard COX-1 inhibitor Ibuprofen with -7.4 kcal/mol interaction affinity. Whereas the compound SAP-26 was found to show the best interaction with the COX-2 receptor (PDB ID:

3LN1) with the interaction affinity of -11.0 kcal/mol which is almost the same as the standard celecoxib with an interaction affinity of -11.1 kcal/mol. Itraconazole was considered the standard drug as the inhibitor of fungal oxidoreductase enzyme (PDB ID: 1AI9). Itraconazole showed the interaction affinity of -10.0 kcal/mol with the receptor, while the compound SAP-28 showed almost the same interaction affinity of -9.6 kcal/mol. The compound Sap-25 showed a very good interaction affinity of -8.9 kcal/mol with the DNA gyrase enzyme of bacteria (PDB ID: 5L3J), whereas metronidazole is being a standard drug showed an interaction affinity of -5.4 kcal/mol. Finally the best compound for the inhibition of TNF-α (PDB ID: 6OP0) was came out as SAP-28 with an interaction affinity -10.0 kcal/mol, while the co-crystal ligand A7A ((R)-{1-[(2,5-dimethylphenyl)methyl]-6-(1-methyl-1H-pyrazol-4-yl)-1H-benzimidazol-2-yl}(pyridin-4-yl)methanol) showed the interaction affinity of -13.7 kcal/mol.

3.2.1. Binding interaction of EGFR with SAP-26 and SAP-28

The *In-silico* molecular docking study between the designed ligands and EGFR protein (PDB ID: 5HG7) directed us towards the two best interaction energy-containing compounds SAP-26 and SAP-28 with the same interaction energy of -9.8 kcal/mol. Both EGFR_SAP-26 complex, as well as EGFR_SAP-28 complex, showed crucial interactions with the receptor as compared to the interactions of standard compound nilotinib with the same receptor (Figure 01). The compound SAP-26 recreated both the π-σ interactions with Leu718 and Leu844 amino acids, as of the standard compound nilotinib. Additionally, SAP-26 showed a π-π stacked interaction with Phe856 amino acid. The compound SAP-28 recreated the π-σ interactions with Leu718 amino acid. Two additional π-π stacked interaction has been observed with Phe723 and Phe856 amino acids. One conventional H-bond was created by the compound with Met793 amino acid.

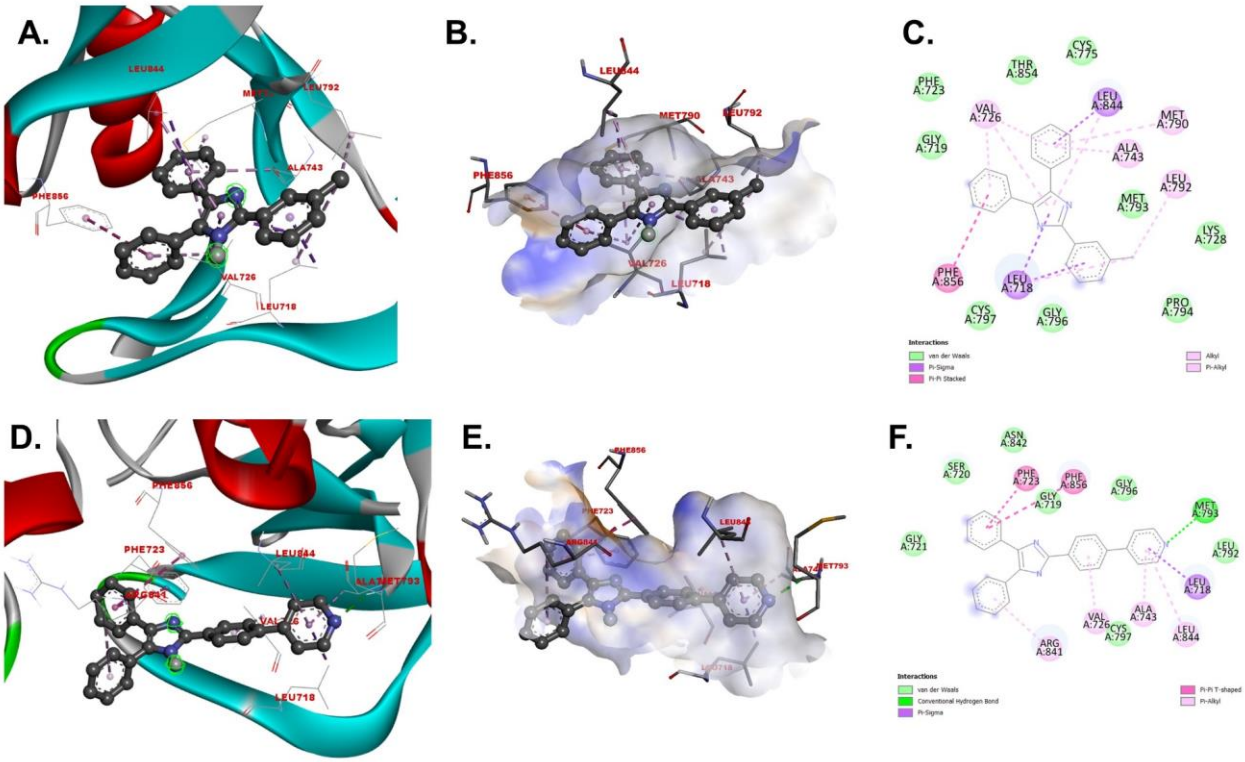

Figure 01. Docking interaction of SAP-26 and SAP-28 with the EGFR protein (PDB ID: 5HG7). A: 3D interaction of the SAP-26 ligand, presented in ball and stick format, with the EGFR receptor, represented as solid ribbon and the interacting amino acids are labelled with red color. B: Compound SAP-26 inside the binding pocket of the receptor. C: 2D interaction of SAP-26 with the EGFR protein. D: 3D interaction of the SAP-28 ligand, presented in ball and stick format, with the EGFR receptor, represented as solid

ribbon and the interacting amino acids are labeled with red color. E: Compound SAP-28 inside the binding pocket of the receptor. F: 2D interaction of the SAP-28 with EGFR protein.

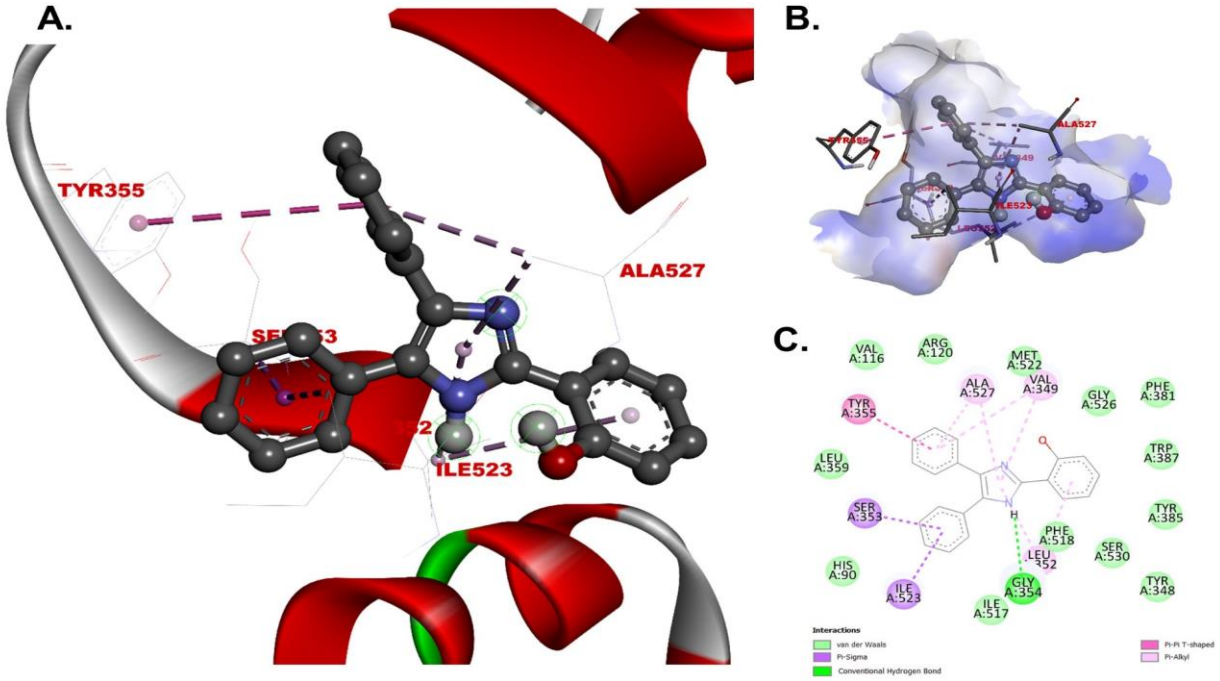

Figure 02. Docking interaction of SAP-19 with the COX-1 protein (PDB ID: 3KK6). A: 3D interaction of the SAP-19 ligand, presented in ball and stick format, with the COX-1 protein, represented as solid ribbon and the interacting amino acids are labelled with red color. B: The compound SAP-19 inside the binding pocket of the protein. C: 2D interaction of SAP-19 with the COX-1 protein.

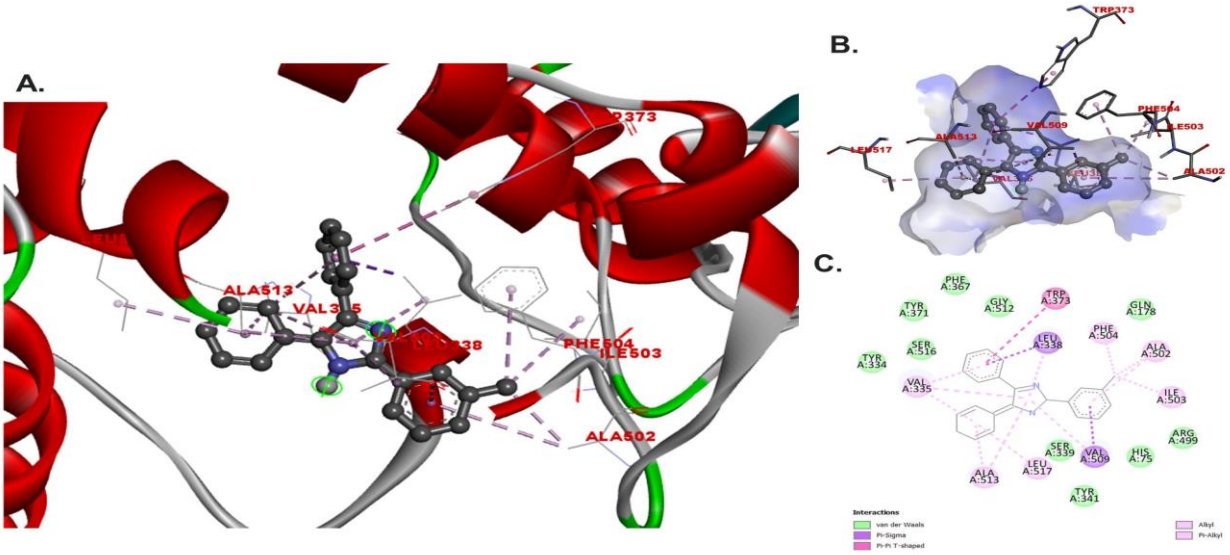

Figure 03. Docking interaction of SAP-26 with the COX-2 protein (PDB ID: 3LN1). A: 3D interaction of the SAP-26 ligand, presented in ball and stick format, with the COX-2 protein, represented as solid ribbon and the interacting amino acids are labelled with red color. B: SAP-26 inside the binding cavity of the COX-2 protein. C: 2D interaction of SAP-26 with the COX-2 protein.

3.3.2. Binding interaction of COX-1 with SAP-19

After the molecular docking studies of all the newly designed compounds with the COX-1 protein (PDB ID: 3KK6), the compound SAP-19 showed the lowest interaction energy of -9.7 kcal/mol. From the COX-1_SAP-19 complex, it was observed that the compound perfectly went inside the binding pocket of the protein and recreated the crucial interaction as compared to the standard molecule

celecoxib (Figure 02). SAP-19 reproduced the π-σ interaction of the standard with Ile523 amino acid, along with an extra π-σ interaction with Ser353 amino acid. The compound SAP-19 also showed similar π-π stacked interaction with Tyr355 amino acid. Finally, the compound was stabilized by a conventional H-bond with Gly354 amino acid.

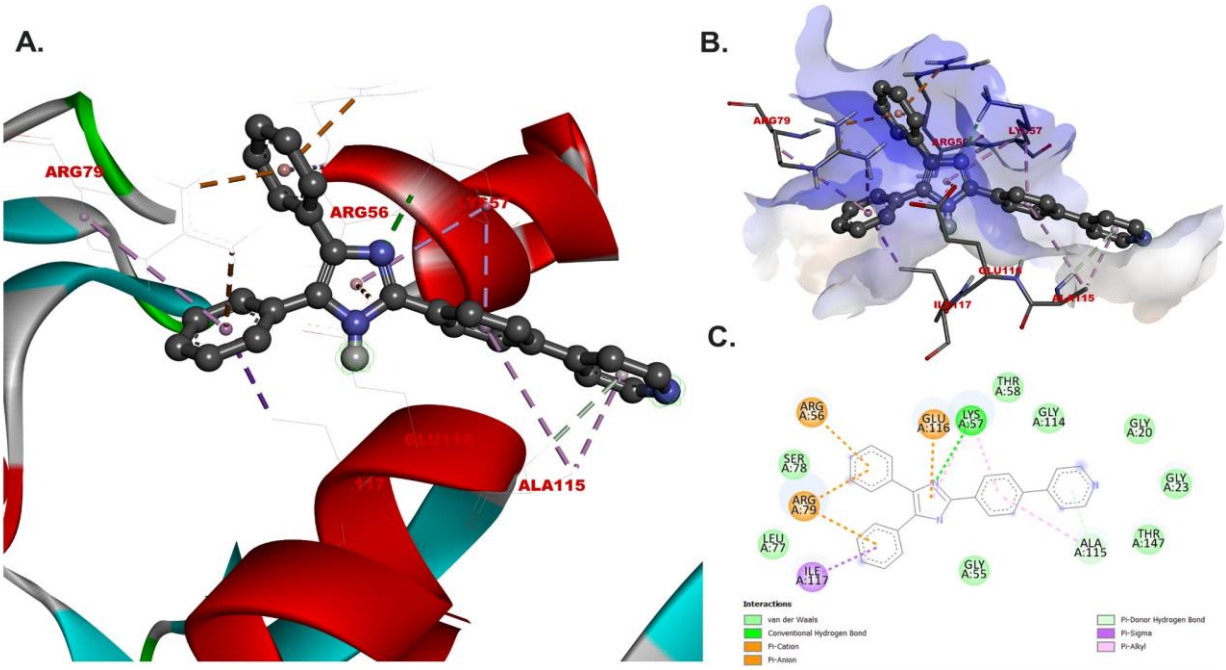

Figure 04. Docking interaction of SAP-28 with the oxidoreductase protein of Candida albicans (PDB ID: 1AI9). A: 3D interaction of the SAP-28 ligand, presented in ball and stick format, with the Oxidoreductase protein, represented in solid ribbon and the interacting amino acids are labelled with red color. B: SAP-28 inside the binding pocket of the receptor. C: 2D interaction of SAP-28 with the oxidoreductase protein.

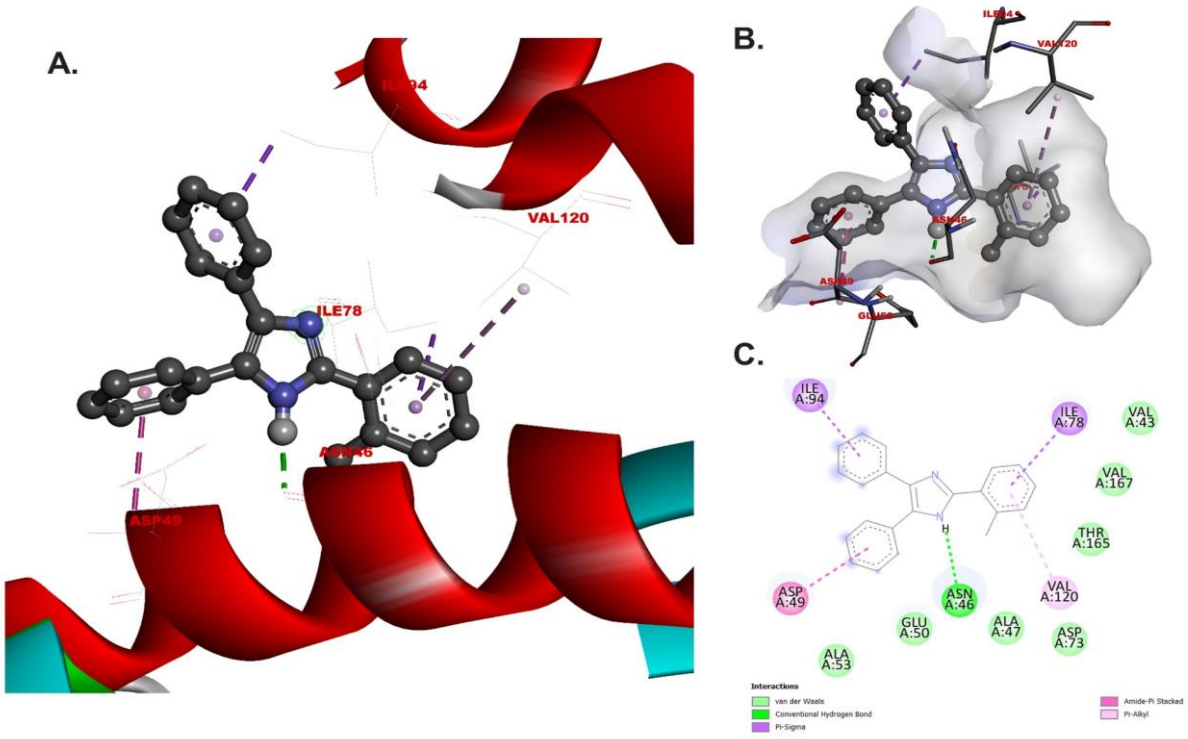

Figure 05. Docking interaction of SAP-25 with the bacterial DNA gyrase (PDB ID: 5L3J). A: 3D interaction of the SAP-25 ligand, presented in ball and stick format, with the DNA gyrase protein,

represented as solid ribbon and the interacting amino acids are labelled with navy blue color. B: SAP-25 inside the biding pocket of the protein. C: 2D interaction of SAP-25 with the DNA gyrase protein.

3.2.3. Binding interaction of COX-2 with SAP-26

With the binding interaction energy of -11.0 kcal/mol, the compound SAP-28 entered deep into the binding pocket of COX-2 protein (PDB ID: 3LN1) (Figure 03). The molecule creates two π-σ interactions with the Val509 and Ser339 amino acids of which the Val509 is a crucial amino acid with respect to celecoxib. The molecule is stabilized by a π-π stacked interaction with Tyr373 amino acid. Other than these interactions, many π-alkyl interactions have been observed with the receptor.

3.2.4. Binding interaction of fungal oxidoreductase with SAP-28

The compound SAP-28 showed good interaction with the oxidoreductase enzyme of the fungus Candida albicans (PDB ID: 1AI9) with an interaction energy of -9.6 kcal/mol. The docked complex of fungal oxidoreductase and SAP-28 revealed that the compound generated a conventional H-bond with Lys57 amino acid through the hydrogen atom, attached to the nitrogen atom of the 3rd position of the imidazole core (Figure 04). The molecule generated four π-cation interactions with Arg56, Arg79, and Glu116 amino acids and got the stabilization. Additionally, one π-σ interaction was observed with the Ile117 amino acid. Many π-alkyl interactions were observed and the compound seemed to be stable in the binding pocket of the receptor.

3.2.5. Binding interaction of bacterial DNA gyrase with SAP-25

The designed compound SAP-25 binds with the bacterial DNA gyrase protein (PDB ID: 5L3J) with very good interaction energy of -8.6 kcal/mol. The protein-ligand complex of bacterial DNA gyrase and SAP-25 revealed that the hydrogen atom at the 1st position of the imidazole produced a conventional H-bond with the crucial amino acid Asn46 (Figure 05). The compound developed π-σ interaction with another crucial amino acid Ile78 as per the standard compound metronidazole. Finally, the compound is stabilized by another π-σ interaction and a π-π stacked interaction with Ile94 and Asp49 respectively.

3.2.6. Binding interaction of Tumor Necrosis Factor-α with SAP-28

The compound SAP-28 showed very good interaction with the TNF-α protein with the binding interaction energy of (-) 10.0 kcal/mol. After analyzing the protein-ligand complex of TNF-α and SAP-28, it was found that the compound went deep inside the binding pocket of the TNF-α protein (Figure 06). All the three crucial π-σ interaction of the co-crystal ligand A7A with Leu57 amino acid of the three chains of the protein was re-generated by SAP-28. The crucial π-π stacked interaction with Tyr56 amino acid was also re-created by the newly designed compound. Additionally, SAP-28 shows a π-anion interaction was found with Leu157 amino acid.

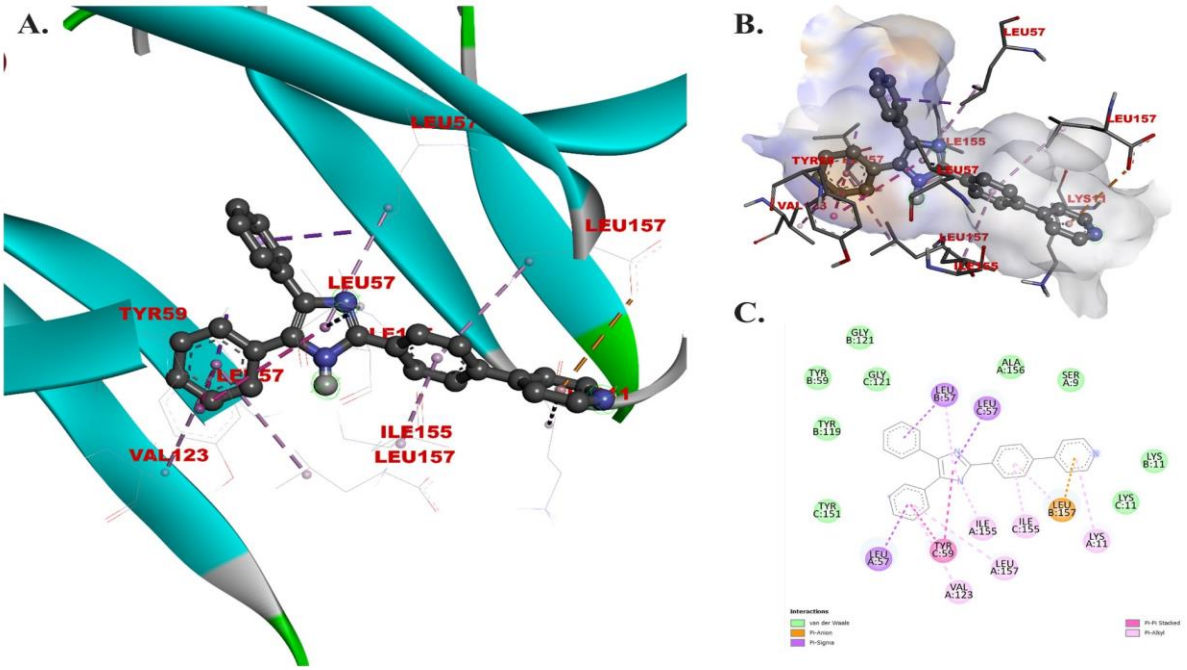

Figure 06. Docking interaction of SAP-28 with the TNF-α protein (PDB ID: 6OP0). A: 3D interaction of the SAP-28 ligand, presented in ball and stick format, with the TNF-α protein, represented as solid ribbon and the

interacting amino acids are labelled with red color. B: SAP-28 inside the binding pocket of the protein. C: 2D interaction of SAP-28 with the TNF-α protein.

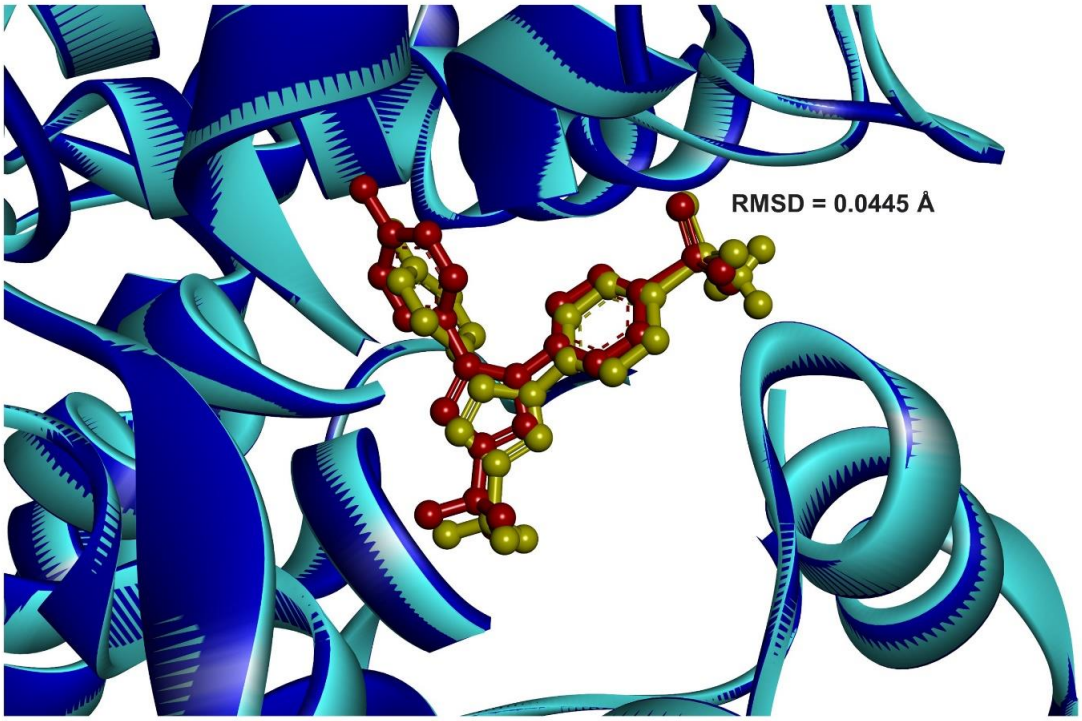

Figure 07. Superimposed image of co-crystal celecoxib molecule and re-docked celecoxib molecule. The co-crystal celecoxib molecule is represented in ball and stick format and in red color. The original protein from PDB file is represented as solid ribbon and in sky blue color. The re-docked celecoxib molecule is represented in ball and stick format and yellow in color. The protein chain of the re-docked complex is represented in solid ribbon format and in navy-blue color.

3.2.7. Validation of molecular docking

The molecular docking protocol was validated by calculating the RMSD values after superimposing the original PDB file and re-docked PDB file with the same ligand. The RMSD of the COX-1 protein was found to be 0.0445 Å (Figure 07). The RMSD of COX-2 protein was found to be 0.0445 Å. The RMSD of the EGFR was found to be 0.0420 Å. The RMSD of fungal oxidoreductase was found to be 0.0498 Å. The RMSD of bacterial DNA gyrase was found 0.0297 Å and for the TNF-α protein, RMSD was 0.399 Å.

3.3. Molecular properties and drug-likeness

The drug-likeness and molecular properties of the top compounds were measured in terms of physicochemical properties, Lipinski's Rule of Five, and Veber's Rule. The top four docked compounds SAP-19, SAP-25, SAP-26, and SAP-28 as well as the compounds with satisfied docking scores SAP-12, SAP-13 and SAP-18 were considered for this evaluation. After evaluation, the parameters of the selected compounds have been reported in Table 3 including the parameters of the five standard compounds nilotinib, celecoxib, itraconazole, metronidazole, and A7A ligand. The molecular weight of all the selected molecules is below 400 g/mol. All the designed molecules contain 3 rotatable bonds except the SAP-28, which has 4 rotatable bonds. The number of H-bond acceptors varies from 1 to 3 which is lower in number compared to the standards (nilotinib has 8 H-bond acceptors). Two H-bond donors are present in the SAP-19, whereas all other designed molecules have 1 H-bond donor which is comparable with all standards (0 to 2 H-bond donors). The total polar surface area of all the compounds is below 50 $Å^2$, which is far below the range of veber's rule parameter (Polar surface area no greater than 140 $Å^2$). The consensus logP (average of all logP) varies from 4.26 to 5.5 which perfectly follows the veber's rule. All the designed compounds have high GI absorption except the SAP-12 along with the nilotinib molecule. The SAP-19, SAP-25, and SAP-26 along with the standard compound A7A showed BBB permeation.

The other 4 compounds are BBB impermeable. All the compounds follow both Lipinski's and Veber's rules.

The first glance of the bioavailability radar of all the top compounds along with standards was represented in Figure 08. The bioavailability radars of the compounds along with the standards are within the saturation range of the radar, which reveals the considerable physicochemical range of the compounds. The insaturation (INSATU) parameter in the bioavailability radar of all the new compounds along with nilotinib, celecoxib, and A7A ligands falls over the saturation level, but within the considerable range (0.25 < Fraction Csp3 < 1). Thus, we can say that all the new compounds have very good bioavailability with respect to the standard drugs.

Table 3. Molecular properties and Drug likeness

Compound Code	MW (g/mol)	Rotatable Bond	H-Bond Acceptor	H-Bond Donor	TPSA (Å^2)	Consensus Log $P_{o/w}$	GI Abs	BBB Permeant	Lipinski's Rule	Veber's Rule
SAP-19	312.36	3	2	2	48.91	4.26	High	Yes	Yes	Yes
SAP-25	310.39	3	1	1	28.68	4.93	High	Yes	Yes	Yes
SAP-26	310.39	3	1	1	28.68	4.92	High	Yes	Yes	Yes
SAP-28	373.45	4	2	1	41.57	5.15	High	No	Yes	Yes
SAP-12	365.26	3	1	1	28.68	5.63	Low	No	Yes	Yes
SAP-13	332.35	3	3	1	28.68	5.21	High	No	Yes	Yes
SAP-18	314.36	3	2	1	28.68	4.90	High	No	Yes	Yes
Nilotinib	529.52	8	8	2	97.62	4.63	Low	No	Yes	Yes
Celecoxib	381.37	4	7	1	86.36	3.40	High	No	Yes	Yes
Itraconazole	705.63	11	7	0	104.70	4.71	High	No	No	No
Metronidazole	171.15	3	4	1	83.87	(-) 0.23	High	No	Yes	Yes
A7A	423.51	5	4	1	68.76	3.6	High	Yes	Yes	Yes

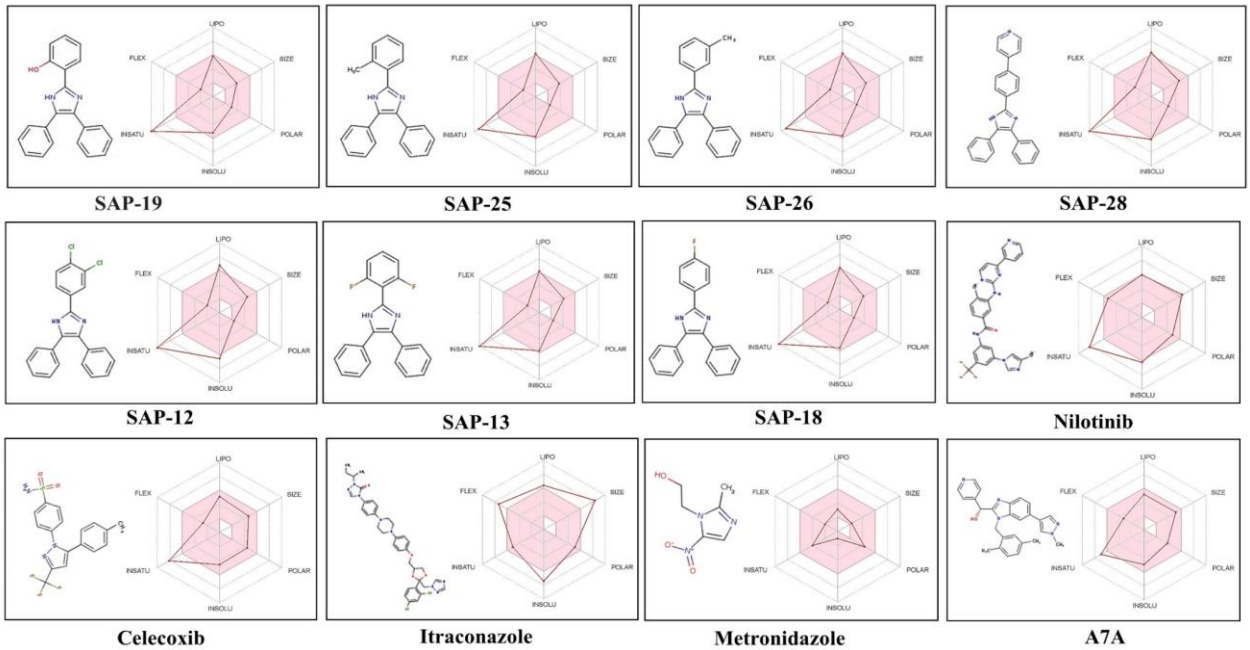

Figure 08. Drug likeness of the top molecule at first glance of bioavailability radar. The pink area represents the optimal range for each property (lipophilicity: XLOGP3 between -0.7 and +5.0, size: MW between 150 and 500 g/mol, polarity: TPSA between 20 and 130 Å^2, solubility: log S not higher than 6, saturation: fraction of carbons in the sp^3 hybridization not less than 0.25, and flexibility: no more than 9 rotatable bonds.

The BoiledEgg representation of the compounds reveals that SAP-13, SAP-18, and SAP-28 along with standard compound celecoxib, itraconazole, and metronidazole have the best ADME parameter

which falls between the GI and BBB (Figure 09), which means that the compounds can easily pass the GI tract and go to the blood circulation but, can't cross the BBB. The compound SAP-12 and the standard drug nilotinib falls very near to the GI border line, which means that the compound is little poor absorbable by the GI tract. The compound SAP-25, SAP-26, and SAP-19 along with the standard compound A7A can cross the BBB and work on brain also.

3.4. Toxicity studies

The toxicity study of all the top docked compounds was checked in the mcule toxicity checker web server (https://mcule.com/apps/toxicity-checker/) and the report revealed that all the compounds are non-toxic in nature. The detailed toxicity studies were carried out on the ProTox-II web server (https://tox-new.charite.de/protox_II/). The result parameters of the toxicity studies are reported in table 4. All the designed top docked compounds are non-hepatotoxic as well as non-carcinogenic in nature. The compounds have a good immunotoxicity nature, which means they can easily pass the immune system of the body and reach the target position like the standards. Though the mutagenicity of the compounds is moderate to a little high, it is comparable with the celecoxib and metronidazole with the value of 0.75 and 0.97 respectively. All the compounds are in a safe range of cytotoxicity. Finally, the lethal dose (LD_{50}) was calculated as 300 mg/kg for all the compounds which are comparable with the itraconazole molecule ((320 mg/kg). The output Toxicity Radar Chart of all the top compounds as well as standard molecules was represented in Figure 10.

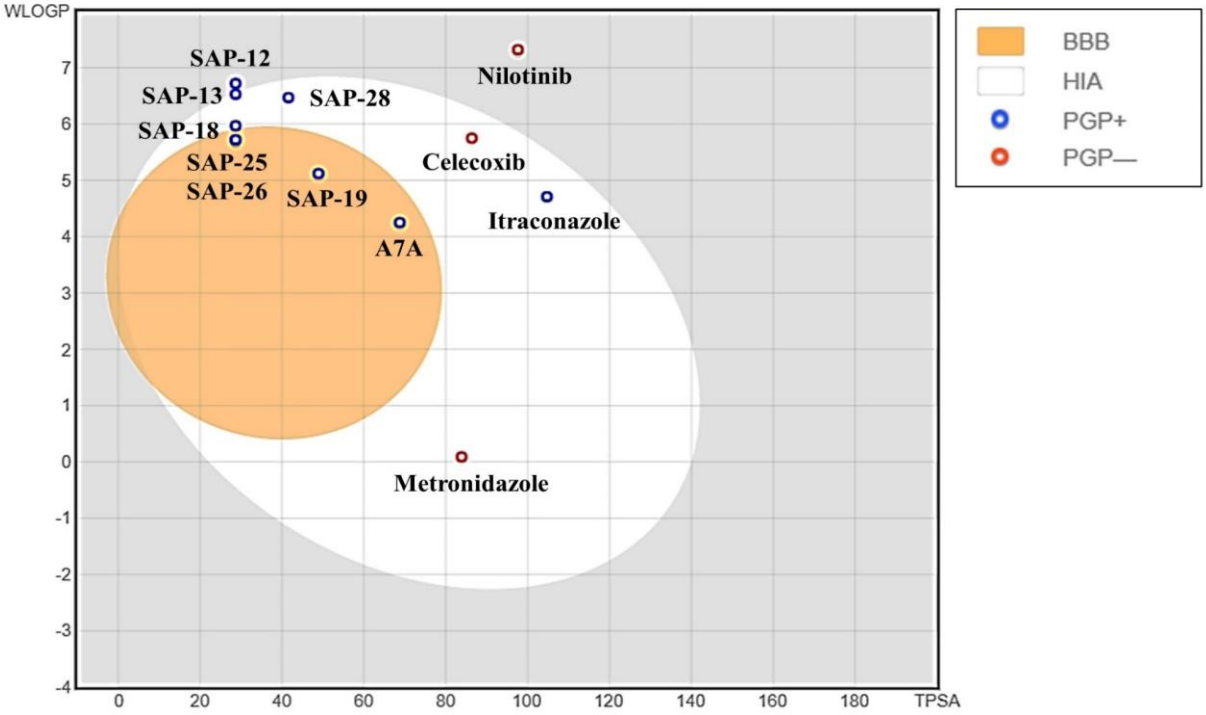

Figure 09. BoiledEgg presentation of the top 7 compounds along with standards. This diagram represents the intuitive evaluation of passive gastrointestinal absorption (HIA) and brain penetration (BBB) in function of the position of the molecules in the WLOGP-versus-TPSA referential.

Table 4. Toxicity Studies of the top docked compounds.

Compound Code	Hepatotoxicity Probability	Carcinogenicity Probability	Immunotoxicity Probability	Mutagenicity Probability	Cytotoxicity Probability	Predicted LD_{50} (mg/kg)
SAP-19	0.57	0.52	0.94	0.70	0.84	300
SAP-25	0.54	0.53	0.98	0.88	0.65	300
SAP-26	0.54	0.53	0.99	0.88	0.88	300
SAP-28	0.50	0.53	0.99	0.82	0.87	300
SAP-12	0.54	0.53	0.99	0.64	0.77	300

SAP-13	0.50	0.50	0.99	0.69	0.74	300
SAP-18	0.50	0.50	0.98	0.69	0.74	300
Nilotinib	0.82	0.53	0.98	0.59	0.72	800
Celecoxib	0.60	0.56	0.99	0.75	0.91	1400
Itraconazole	0.88	0.62	0.75	0.53	0.90	320
Metronidazole	0.87	0.87	0.95	0.97	0.88	1500
A7A	0.71	0.54	0.83	0.55	0.61	700

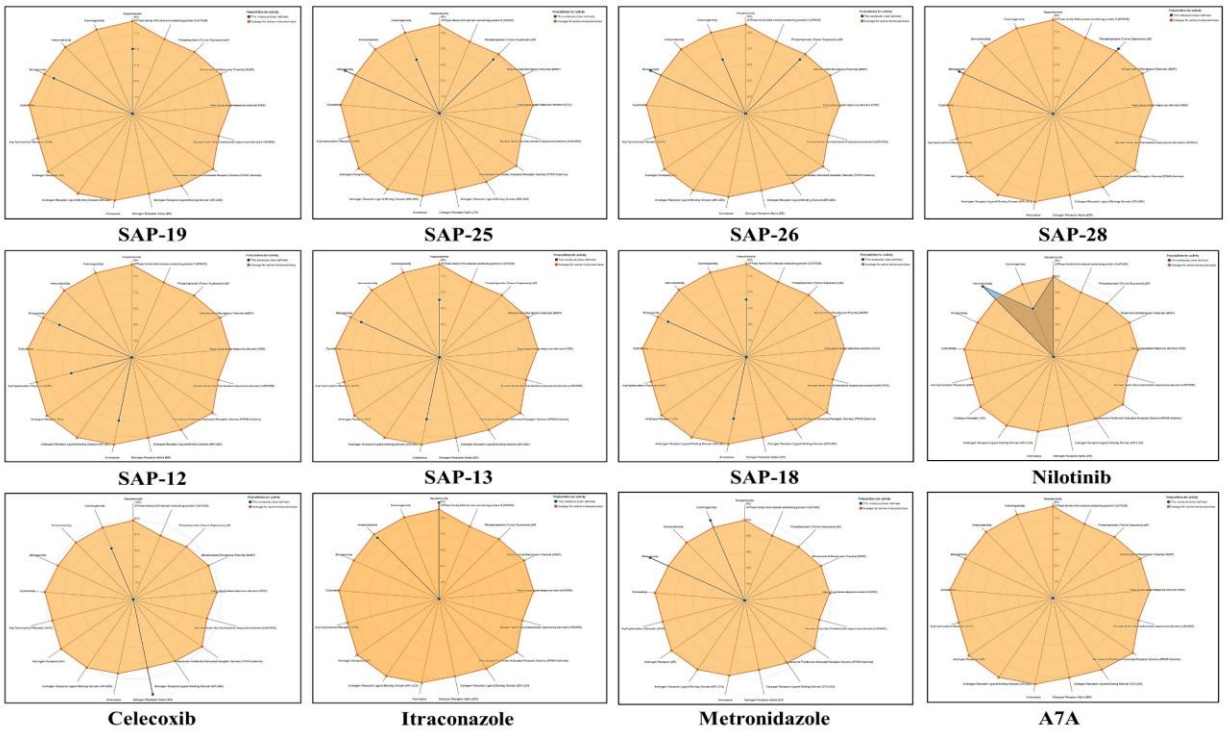

Figure 10. Toxicity Radar Chart of the top compounds with standards. Probabilities for average activity of active molecules/class are denoted by orange dots which forms the toxicity radar. The current molecule (molecule to be evaluated) is denoted by blue points.

Table 5. Kinase inhibitor scores of the top hit compounds.

Compound Code	Kinase inhibitor	Compound Code	Kinase inhibitor
SAP-19	0.38	SAP-12	0.36
SAP-25	0.41	SAP-13	0.52
SAP-26	0.37	SAP-18	0.42
SAP-28	0.46	Nilotinib	0.63

3.5. Biological activity prediction

The *In-silico* kinase inhibition of the top compounds along with standard (nilotinib) were re-verified through the Molinspiration Cheminformatics Software webserver (https://www.molinspiration.com/), which revealed that all the top docked compounds have very good kinase inhibitor activity (Table 5). Though the new designed molecules showed lower kinase inhibition value than that of nilotinib, the values are satisfactory as nilotinib is a very potent kinase inhibitor.

Further, detailed perdition of the probable target for the top docked compounds was checked in the SwissTargetPrediction web server (http://www.swisstargetprediction.ch/index.php). The result reviled that compounds SAP-25 and SAP-26 among all compounds have 8 different target activities (Figure 11). The compound SAP-12 and SAP-19 are active against 7 different targets. The SAP-13, SAP-18 and SAP-28 have very prominent kinase activity.

3.6. MD Simulation analysis

The stability of all the top docked compounds with their respective receptor protein was checked by the MD simulation studies for 100 ns. In this time interval different trajectories like RMSD, Rg, RMSF and H-bonding were analysed (Figure. 12-16.).

The root mean square deviation (RMSD) determines the stability of the protein-ligand complex by assessing the equilibration period of the MD run and denoting the dynamical changes of protein as well as a ligand at a particular temperature, pressure, throughout the simulation time. For the protein as well as the ligand the RMSD analysis was performed (Figure 12 and Figure 13). For the compound SAP-26 and EGFR (PDB ID: 5HG7), the complex the RMSD varies from 0.21 nm to 0.34 nm with an average of 0.28 nm, while the ligand (SAP-26) RMSD varies from 0.62 nm to 0.8 nm with an average of 0.71 nm with no instability observed.

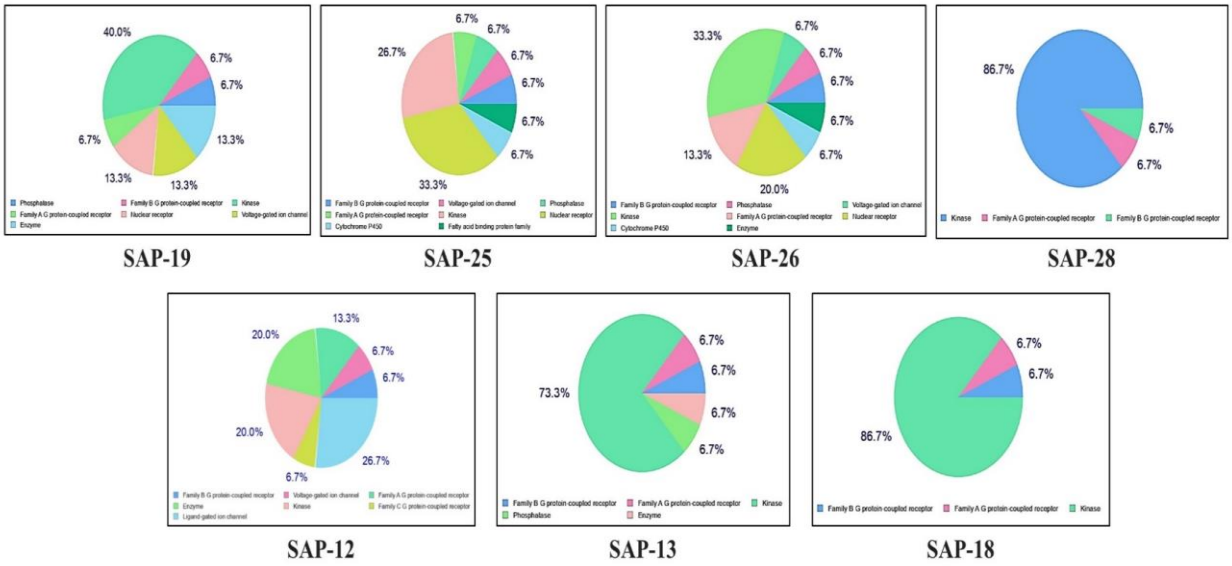

Figure 11. Target prediction of the top hit compounds. The predicted target for the top molecules are denoted by specific color with the probable %.

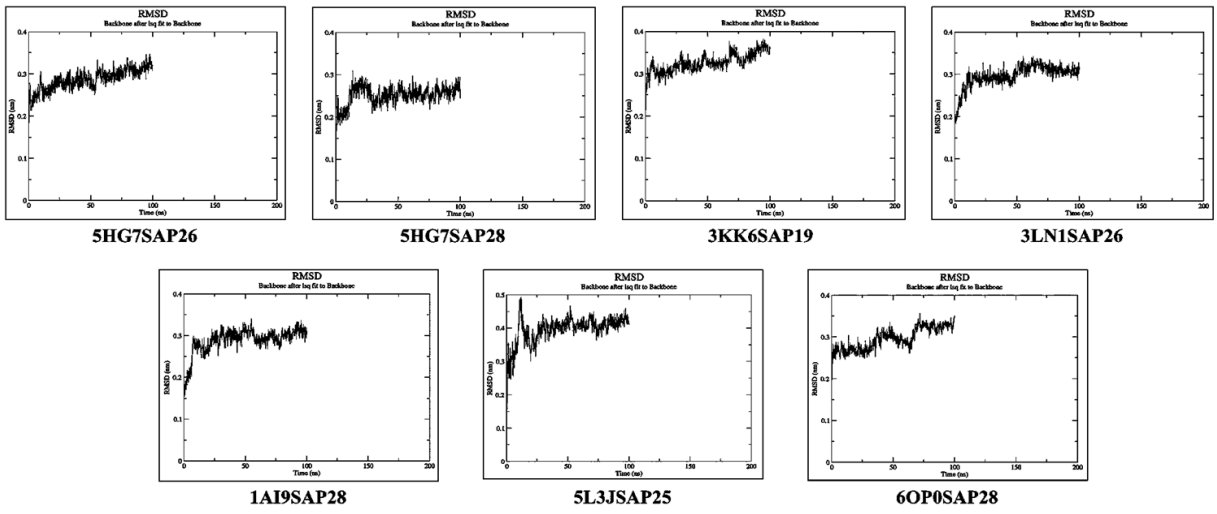

Figure 12. The root mean square deviation (RMSD) of the backbone (protein) in protein-ligand complexes of top compounds.

The same protein with compound SAP-28 complex showed RMSD from 0.18 nm to 0.28 nm with an average of 0.23 nm with no major instability, while the ligand (SAP-28) RMSD varies from 0.2 nm to 0.4 nm with an average of 0.3 nm with no instability in the trajectory. For the COX-1 protein (PDB ID: 3KK6) and SAP-19 complex, the RMSD varies from 0.28 nm to 0.38 nm with an average of 0.33

nm with no instability, while the ligand (SAP-19) RMSD varies from 0.23 nm to 0.38 nm with an average of 0.305 nm. The COX-2 protein (PDB ID: 3LN1) and SAP-26 complex showed the RMSD varies from 0.2 nm to 0.34 nm with an average of 0.27 nm, while the ligand (SAP-26) RMSD varies from 0.3 nm to 0.6 nm with an average of 0.45 nm with no instability in the MD run time. The fungal oxidoreductase protein (PDB ID: 1AI9) with the compound SAP-28 complex showed the RMSD from 0.2 nm to 0.34 nm with an average of 0.27 nm, while the ligand (SAP-28) RMSD varies from 0.35 nm to 0.55 nm with an average of 0.45 nm with no instability in the trajectory. The bacterial DNA gyrase protein (PDB ID: 5L3J) with its top docked ligand SAP-25 showed the RMSD varies from 0.25 nm to 0.48 nm with an average of 0.37 nm, while the ligand (SAP-25) RMSD varies from 0.3 nm to 0.8 nm with minor instability till 60 ns and after that, it got stabilized. The TNF-α protein (PDB ID: 6OP0) with its top docked compound SAP-28 complex showed RMSD from 0.25 nm to 0.34 nm with an average of 0.3 nm, while the ligand (SAP-28) RMSD varied from 0.2 nm to 0.35 nm with an average of 0.28 nm with no instability in the trajectory. All the compounds along with their respective receptor seem to be stable as the no major RMSD instability in the 100 ns MD runtime.

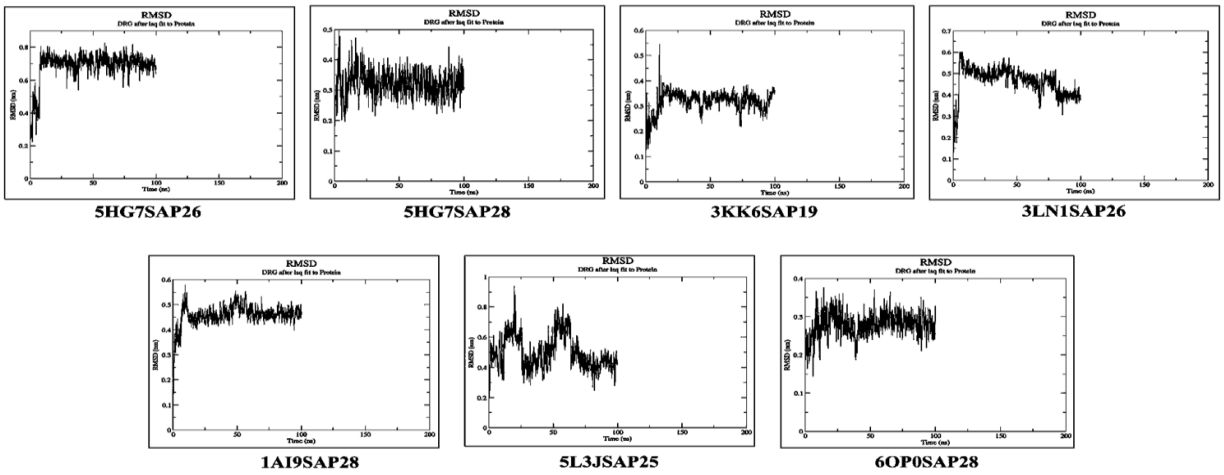

Figure 13. The root mean square deviation (RMSD) of the ligands in protein-ligand complexes of top compounds.

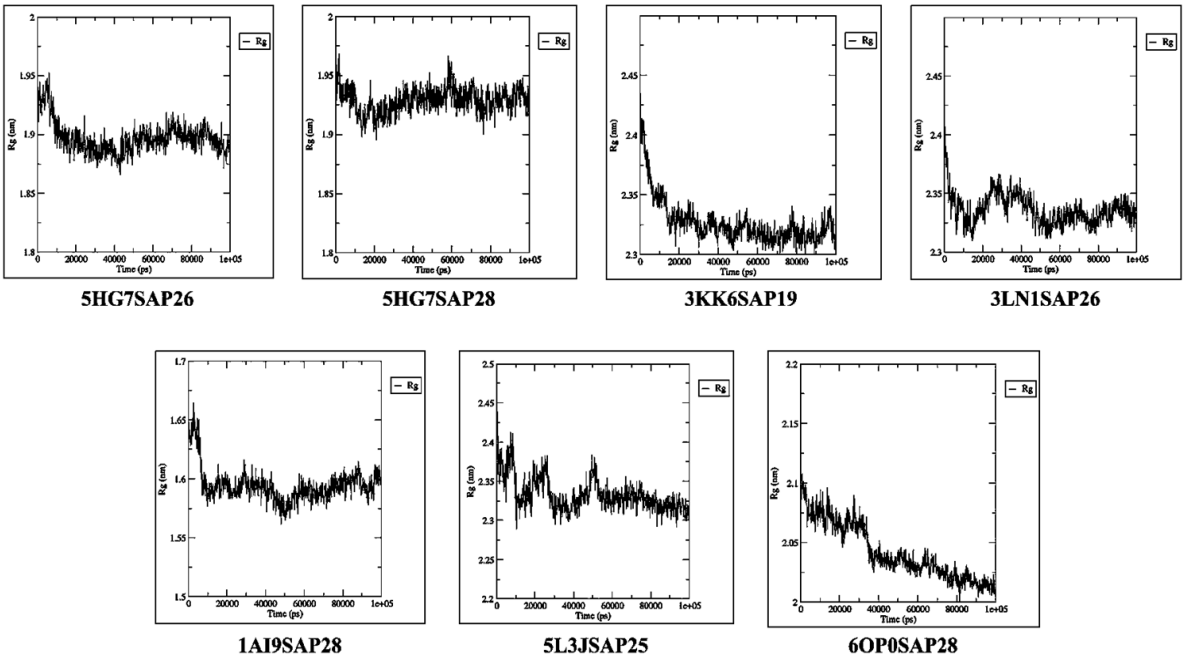

Figure 14: The radius of gyration (Rg) of the top compounds in the protein-ligand complexes.

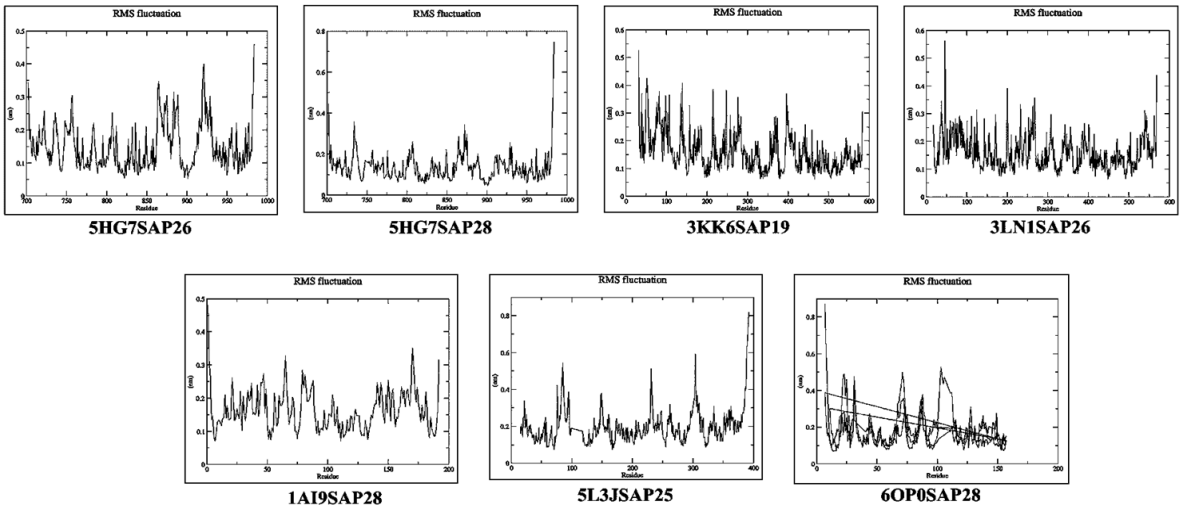

Figure 15: The root mean square fluctuation (RMSF) of the protein-ligand complexes through 100 ns run time.

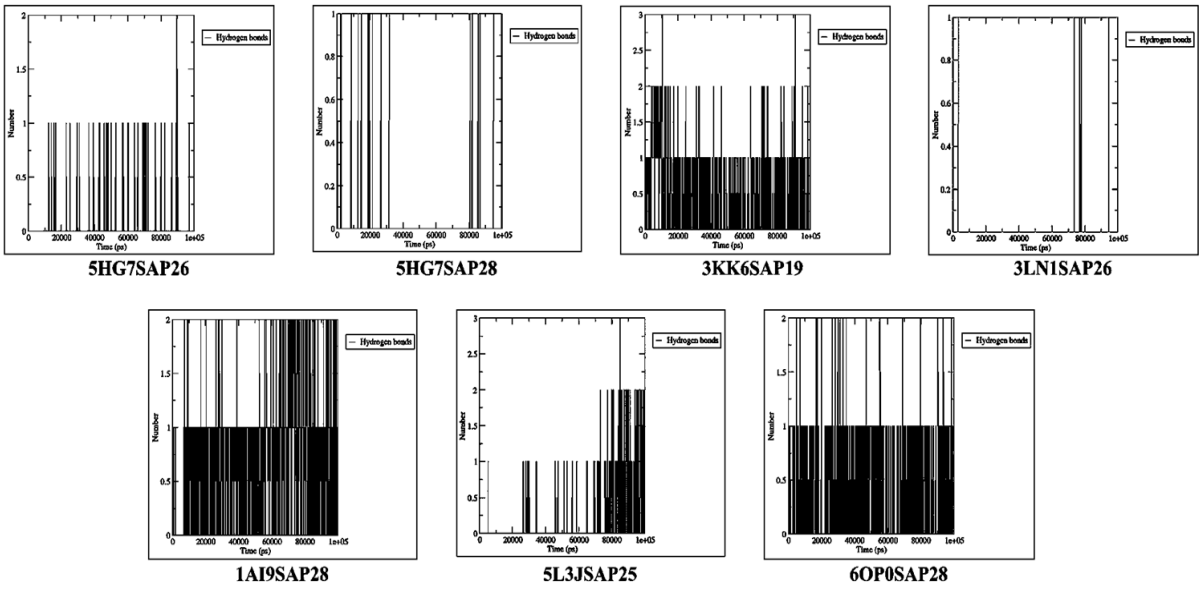

Figure 16: H-bonds of the top compound containing protein-ligand complexes through 100 ns run time.

The root mean square fluctuation (RMSF) determines the fluctuation in the residues or local changes of a protein-ligand complex at isothermic and isobaric processes. The larger the range of fluctuations and/or the number of residues engaged in fluctuation, the worse the ligand and protein binding, and the more likely the ligand and protein will dissociate from the binding site throughout the MD simulation run time (Figure 15). The RMSF of EGFR and SAP-26 was found to be distributed between 0.07 nm to 0.3 nm with no major fluctuation, while the RMSF of SAP-28 with the same protein is distributed between 0.07 nm to 0.33 nm with no fluctuation in the whole run time. The RMSF of COX-1 protein with SAP-19 is distributed between 0.06 nm to 0.4 nm with no major fluctuations. The COX-2 protein with SAP-26 showed the RMSF in the range of 0.09 nm to 0.35 nm with no fluctuations. The fungal oxidoreductase protein with SAP-28 showed the RMSF varies from 0.08 nm to 0.3 nm with minor fluctuation near residue no 75. The DNA gyrase protein of bacteria along with the SAP-25 showed the RMSF value varied from 0.07 nm to 0.45 nm with minor fluctuation near residue no 80. The RMSF of TNF-α with the compound SAP-28 was found to be distributed between 0.07 nm to 0.43 nm with minor fluctuations near residues no 25 and

110. The protein TNF-α is composed of three chains of amino acids and all three chains have their attributions in the binding pocket. Thus three parallel lines can be seen in the RMSF graph. As no major fluctuations are observed in the RMSF trajectories of all the protein-ligand complexes, thus it can be said that the complex was stable throughout the 100 ns runtime.

For the prediction of the stability of the protein-ligand complex, the determination of the hydrogen bond is very essential as it is the strongest bond between the protein and the ligand. Thus, we can say more the number of H-bond, the more is the stability of the complex in the MD simulation runtime (Figure 16).

Table 6. Pharmacophoric features of all the top compounds in the top score model.

SL NO	Molecule	Atoms	Features	Spatial Features	Aromatic	Hydrophobic	Donors	Acceptors	Negatives	Positives
1	SAP-13	39	7	6	4	0	1	1	0	1
2	SAP-19	40	9	7	4	0	2	2	0	1
3	SAP-26	41	8	7	4	1	1	1	0	1
4	SAP-25	41	8	7	4	1	1	1	0	1
5	SAP-18	39	7	6	4	0	1	1	0	1
6	SAP-28	48	9	8	5	0	1	2	0	1
7	SAP-12	39	7	6	4	0	1	1	0	1

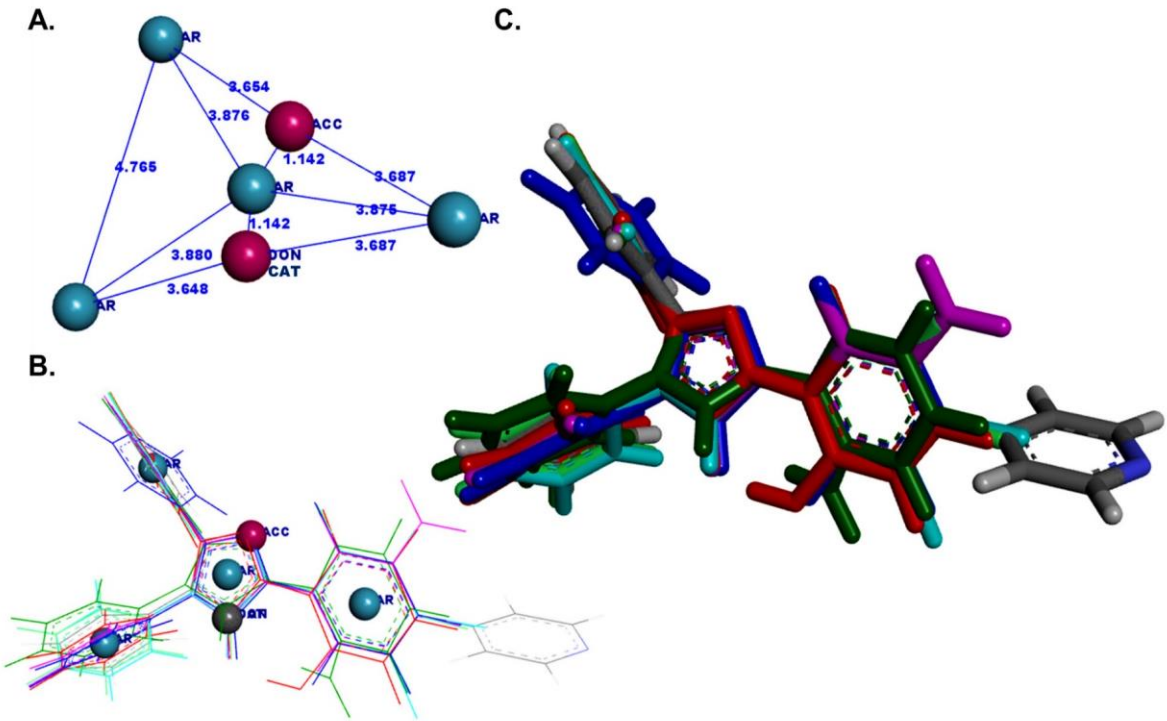

Figure 17: Pharmacophore mapping of the top compounds. A: Common pharmacophoric feature of all the compounds. B: Superimposition of all molecules with the pharmacophoric features. C: Molecular overlay of all the top compounds.

The EGFR protein with SAP-26 showed 0 to 1 H-bond with an average of 0.5 H-bond, whereas the same protein with SAP-28 showed a similar 0 to 1 H-bond with an average of 0.5 H-bond. The docked protein-ligand complex showed 0 and 1 H-bond respectively which is similar to the MD results. The COX-1 protein with SAP-19 showed 0 to 2 H-bonds with an average of 1 H-bond, which perfectly matches with the docked complex. The COX-2 protein with SAP-26 showed 0 to 0.5 H-bond with an average of 0.25 H-bond, which matched with the absence of H-bond in the docked complex. The fungal oxidoreductase enzyme complex with SAP-28 showed 0 to 2 H-bonds with an average of 1 H-

bond which matched with the 1 H-bond of the docked complex. The DNA gyrase enzyme complex with SAP-25 showed 0 to 2 H-bond with an average of 1 H-bond which perfectly matches with the 1 H-bond in the docked complex. The TNF-α protein with SAP-28 showed 0 to 1 H-bond with an average 0.5 H-bond, whereas the docked complex showed no H-bond which resembles the MD simulation results.

3.7. Pharmacophore mapping

The pharmacophores of a molecule are group of key functional or structural characteristics that are thought to be responsible for the molecule's biological activity involving interactions with the active site residues of the biological target. The common pharmacophore was generated through the PharmaGist web server (https://bioinfo3d.cs.tau.ac.il/PharmaGist/php.php) . The best pharmacophore matching score was obtained as 47.829. Aromatic, Hydrophobic, H-bond Donors, H-bond Acceptors, Negatives and Positives features were calculated for all the top 7 compounds (Table 6). The result revealed that 4 aromatic ring, 1 H-bond donor, 1 H-bond acceptor, and 1 positive feature is present in the common pharmacophore. The distance between the ring aromatic features should be 4.766 Å, 3.876 Å, 3.880 Å, 3.875 Å respectively (Figure 17A). The distance between the middle ring aromatic feature and the acceptor as well as the donor feature should be 1.142 Å. The positive charge feature is overlapped with the H-bond donor feature as both are in the same position.

4. Conclusions

The new lophine moiety is very less exposed to the world of pharmaceuticals. The chemiluminescence property of the lophine moiety has been reported by many scientists. Based on the reported activity of imidazole moiety and randomized addition of different functional groups, different derivatives of the lophine was designed. The designed derivatives of lophine moiety showed potential activity as anti-cancer, anti-inflammatory, anti-fungal, anti-viral molecules and a potential inhibitor of TNF-α protein. The compound SAP-28 with a pyridine substitution at the para position of the phenyl ring present at the 2nd position of the imidazole makes it a potential moiety against EGFR, viral oxidoreductase protein and TNF-α protein. The compound SAP-26 came out as potential EGFR and COX-2 inhibition activity for the presence of a methyl group at the meta-position of the phenyl ring at the 2nd position of imidazole. The compound SAP-25 with a methyl group at the ortho-position of the 2nd position phenyl ring of the imidazole core. The SAP-19 showed potential COX-1 inhibition for the presence of a hydroxyl group at the ortho-position of the phenyl group present at the 2nd position of imidazole. Along with this the compound SAP-12, SAP-13 and SAP-18 had come out with satisfactory docking analysis results. All the designed top docked compounds follow Lipinski's rule of five as well as Veber's rule along with good GI absorption capability. The compounds SAP-19, SAP-25 and SAP-26 showed the BBB permeability and further can be developed for brain tumour treatment. The toxicological parameters say that all the compounds are in a safe zone for use with an LD_{50} of 300mg/kg/day. All the top compounds showed potent kinase inhibition activity. Finally, the MD simulation studies confirmed the receptor-ligand stability of the compounds. There are needed four aromatic ring centres with an H-bond donor and an H-bond acceptor group along with a positive ionisable group in the pharmacophoric structure of the compounds.

This *In-silico* study established that, various substitution on the phenyl ring present in the 2nd position of the imidazole such as 2-hydroxy, 2-methyl, 3-methyl, 4-pyridinyl etc. governing their ability to interact with diverse targets. For example introduction of 2-hydroxy group proved to be beneficial for COX-1 inhibition activity whereas, incorporation of 3-methyl group displayed COX-2 inhibition activity. Introduction of 2-methyl and 4-pyridinyl group govern the anti-bacterial, anti-fungal, anticancer and TNF-α inhibitor. Organic chemist are encouraged to perform diverged synthetic pathway of lophine derivatives and to develop new lead molecules for the control and eradication of various diseases. More studies on lophine must be explored for rational drugs designs and development.

Acknowledgements

The authors are thankful to CIPT & AHS, Howrah; ABMRCP, Bengaluru; Flemming College of

Pharmacy, Kolkata and The Neotia University, South 24 Parganas for all the supports.

Abbreviations

COX: Cyclooxygenase, LOX: Lipoxygenase, MAPK: Mitogen-Activated Protein Kinase, EGFR: Epidermal Growth Factor Receptor, TNF-α: Tumour Necrosis Factor-alpha, PAMPs: Pathogen-Associated Molecular Patterns, DAMPs: Danger-Associated Molecular Patterns, ADME: Absorption Distribution Metabolism and Excretion, PDB: Protein Data Bank, RCSB: Research Collaboratory for Structural Bioinformatics, SMILES: Simplified Molecular-Input Line-Entry System, GROMACS: GROningen MAchine for Chemical Simulations, MD Simulations: Molecular Dynamics Simulations

References

[1] H. WALBA, R.W. ISENSEE, Acidity Constants of Some Arylimidazoles and Their Cations, J Org Chem 26 (1961) 2789–2791. https://doi.org/10.1021/jo01066a039.

[2] Adel A. Marzouk, Vagif. M. Abbasov, Avtandil H. Talybov, Shaaban Kamel Mohamed, Synthesis of 2,4,5-Triphenyl Imidazole Derivatives Using Diethyl Ammonium Hydrogen Phosphate as Green, Fast and Reusable Catalyst, World Journal of Organic Chemistry 1 (2013) 6–10.

[3] P. Sharma, C. LaRosa, J. Antwi, R. Govindarajan, K.A. Werbovetz, Imidazoles as Potential Anticancer Agents: An Update on Recent Studies, Molecules 26 (2021) 4213. https://doi.org/10.3390/molecules26144213

[4] M. Bolous, N. Arumugam, A.I. Almansour, R. Suresh Kumar, K. Maruoka, V.C. Antharam, S. Thangamani, Broad-spectrum antifungal activity of spirooxindolo-pyrrolidine tethered indole/imidazole hybrid heterocycles against fungal pathogens, Bioorg Med Chem Lett 29 (2019) 2059–2063. https://doi.org/10.1016/j.bmcl.2019.07.022.

[5] W.A. Toscano, D.R. Storm, Bacitracin, Pharmacol Ther 16 (1982) 199–210. https://doi.org/10.1016/0163-7258(82)90054-7.

[6] O.S. Adeyemi, A.O. Eseola, W. Plass, O. Atolani, T. Sugi, Y. Han, G.E. Batiha, K. Kato, O.J. Awakan, T.D. Olaolu, C.O. Nwonuma, O. Alejolowo, A. Owolabi, D. Rotimi, O.T. Kayode, Imidazole derivatives as antiparasitic agents and use of molecular modeling to investigate the structure–activity relationship, Parasitol Res 119 (2020) 1925–1941. https://doi.org/10.1007/s00436-020-06668-6.

[7] J.A. Jablonowski, K.S. Ly, M. Bogenstaetter, C.A. Dvorak, J.D. Boggs, L.K. Dvorak, B. Lord, K.L. Miller, C. Mazur, S.J. Wilson, T.W. Lovenberg, N.I. Carruthers, Novel imidazole-based histamine H3 antagonists, Bioorg Med Chem Lett 19 (2009) 903–907. https://doi.org/10.1016/j.bmcl.2008.11.114.

[8] M. Mor, F. Bordi, C. Silva, S. Rivara, V. Zuliani, F. Vacondio, G. Morini, E. Barocelli, V. Ballabeni, M. Impicciatore, P.V. Plazzi, Synthesis and biological assays of new H3-antagonists with imidazole and imidazoline polar groups, Il Farmaco 55 (2000) 27–34. https://doi.org/10.1016/S0014-827X(99)00115-9.

[9] A.-R.A. Al-Majed, E. Assiri, N.Y. Khalil, H.A. Abdel-Aziz, Losartan, in: 2015: pp. 159–194. https://doi.org/10.1016/bs.podrm.2015.02.003.

[10] K. Nikolic, D. Agbaba, Imidazoline Antihypertensive Drugs: Selective I1-Imidazoline Receptors Activation, Cardiovasc Ther 30 (2012) 209–216. https://doi.org/10.1111/j.1755-5922.2011.00269.x.

[11] G. Navarrete-Vázquez, S. Hidalgo-Figueroa, M. Torres-Piedra, J. Vergara-Galicia, J.C. Rivera-Leyva, S. Estrada-Soto, I. León-Rivera, B. Aguilar-Guardarrama, Y. Rios-Gómez, R. Villalobos-Molina, Synthesis, vasorelaxant activity and antihypertensive effect of benzo[d]imidazole derivatives, Bioorg Med Chem 18 (2010) 3985–3991. https://doi.org/10.1016/j.bmc.2010.04.027.

[12] A. Puratchikody, M. Doble, Antinociceptive and antiinflammatory activities and QSAR studies on 2-substituted-4,5-diphenyl-1H-imidazoles, Bioorg Med Chem 15 (2007) 1083–1090. https://doi.org/10.1016/j.bmc.2006.10.025.

[13] M.V.P.S. Nascimento, A.C.M. Munhoz, L.C. Theindl, E.T.B. Mohr, N. Saleh, E.B. Parisotto, T.A. Rossa, A. Zamoner, T.B. Creczynski-Pasa, F.B. Filippin-Monteiro,

M.M. Sá, E.M. Dalmarco, A Novel Tetrasubstituted Imidazole as a Prototype for the Development of Anti-inflammatory Drugs, Inflammation 41 (2018) 1334–1348. https://doi.org/10.1007/s10753-018-0782-y.

[14] G.L. Sasahara, F.S. Gouveia Júnior, R. de O. Rodrigues, D.S. Zampieri, S.G. da C. Fonseca, R. de C.R. Gonçalves, B.R. Athaydes, R.R. Kitagawa, F.A. Santos, E.H.S. Sousa, A.T. Nagao-Dias, L.G. de F. Lopes, Nitro-imidazole-based ruthenium complexes with antioxidant and anti-inflammatory activities, J Inorg Biochem 206 (2020) 111048. https://doi.org/10.1016/j.jinorgbio.2020.111048.

[15] L. Zhang, X.-M. Peng, G.L. v. Damu, R.-X. Geng, C.-H. Zhou, Comprehensive Review in Current Developments of Imidazole-Based Medicinal Chemistry, Med Res Rev 34 (2014) 340–437. https://doi.org/10.1002/med.21290.

[16] N. Fridman, M. Kaftory, Y. Eichen, S. Speiser, Spectroscopy, photophysical and photochemical properties of bisimidazole derivatives, J Photochem Photobiol A Chem 188 (2007) 25–33. https://doi.org/10.1016/j.jphotochem.2006.11.014.

[17] D. Yanover, M. Kaftory, Lophine (2,4,5-triphenyl-1 H -imidazole), Acta Crystallogr Sect E Struct Rep Online 65 (2009) o711–o711. https://doi.org/10.1107/S1600536809006552.

[18] E.H. White, M.J.C. Harding, The Chemiluminescence of Lophine and Its Derivatives, J Am Chem Soc 86 (1964) 5686–5687. https://doi.org/10.1021/ja01078a062.

[19] K. Nakashima, Lophine derivatives as versatile analytical tools, Biomedical Chromatography 17 (2003) 83–95. https://doi.org/10.1002/bmc.226.

[20] J.S. da Costa, J.P.B. Lopes, D. Russowsky, C.L. Petzhold, A.C. de A. Borges, M.A. Ceschi, E. Konrath, C. Batassini, P.S. Lunardi, C.A.S. Gonçalves, Synthesis of tacrine-lophine hybrids via one-pot four component reaction and biological evaluation as acetyl- and butyrylcholinesterase inhibitors, Eur J Med Chem 62 (2013) 556–563. https://doi.org/10.1016/j.ejmech.2013.01.029.

[21] J.P.B. Lopes, L. Silva, M.A. Ceschi, D.S. Lüdtke, A.R. Zimmer, T.C. Ruaro, R.F. Dantas, C.M.C. de Salles, F.P. Silva-Jr, M.R. Senger, G. Barbosa, L.M. Lima, I.A. Guedes, L.E. Dardenne, Synthesis of new lophine–carbohydrate hybrids as cholinesterase inhibitors: cytotoxicity evaluation and molecular modeling, Medchemcomm 10 (2019) 2089–2101. https://doi.org/10.1039/C9MD00358D.

[22] D.N. Granger, E. Senchenkova, Inflammation and the Microcirculation, Colloquium Series on Integrated Systems Physiology: From Molecule to Function 2 (2010) 1–87. https://doi.org/10.4199/C00013ED1V01Y201006ISP008.

[23] S.K. Biswas, Does the Interdependence between Oxidative Stress and Inflammation Explain the Antioxidant Paradox?, Oxid Med Cell Longev 2016 (2016) 1–9. https://doi.org/10.1155/2016/5698931.

[24] G.W. Schmid-Schönbein, ANALYSIS OF INFLAMMATION, Annu Rev Biomed Eng 8 (2006) 93–151. https://doi.org/10.1146/annurev.bioeng.8.061505.095708.

[25] M.V.P.S. Nascimento, A.C.M. Munhoz, L.C. Theindl, E.T.B. Mohr, N. Saleh, E.B. Parisotto, T.A. Rossa, A. Zamoner, T.B. Creczynski-Pasa, F.B. Filippin-Monteiro, M.M. Sá, E.M. Dalmarco, A Novel Tetrasubstituted Imidazole as a Prototype for the Development of Anti-inflammatory Drugs, Inflammation 41 (2018) 1334–1348. https://doi.org/10.1007/s10753-018-0782-y.

[26] P.S. Roy, B.J. Saikia, Cancer and cure: A critical analysis., Indian J Cancer 53 (2016) 441–442. https://doi.org/10.4103/0019-509X.200658.

[27] P. Blume-Jensen, T. Hunter, Oncogenic kinase signalling, Nature 411 (2001) 355–365. https://doi.org/10.1038/35077225.

[28] A. Ullrich, J. Schlessinger, Signal transduction by receptors with tyrosine kinase activity, Cell 61 (1990) 203–212. https://doi.org/10.1016/0092-8674(90)90801-K.

[29] N.E. Hynes, H.A. Lane, ERBB receptors and cancer: the complexity of targeted inhibitors,

Nat Rev Cancer 5 (2005) 341–354. https://doi.org/10.1038/nrc1609.

[30] M. Scaltriti, J. Baselga, The Epidermal Growth Factor Receptor Pathway: A Model for Targeted Therapy: Fig. 1., Clinical Cancer Research 12 (2006) 5268–5272. https://doi.org/10.1158/1078-0432.CCR-05-1554.

[31] Y. Yarden, M.X. Sliwkowski, Untangling the ErbB signalling network, Nat Rev Mol Cell Biol 2 (2001) 127–137. https://doi.org/10.1038/35052073.

[32] R. Butti, S. Das, V.P. Gunasekaran, A.S. Yadav, D. Kumar, G.C. Kundu, Receptor tyrosine kinases (RTKs) in breast cancer: signaling, therapeutic implications and challenges, Mol Cancer 17 (2018) 34. https://doi.org/10.1186/s12943-018-0797-x.

[33] J.L. Macdonald-Obermann, L.J. Pike, Different Epidermal Growth Factor (EGF) Receptor Ligands Show Distinct Kinetics and Biased or Partial Agonism for Homodimer and Heterodimer Formation, Journal of Biological Chemistry 289 (2014) 26178–26188. https://doi.org/10.1074/jbc.M114.586826.

[34] S. Sigismund, D. Avanzato, L. Lanzetti, Emerging functions of the <scp>EGFR</scp> in cancer, Mol Oncol 12 (2018) 3–20. https://doi.org/10.1002/1878-0261.12155.

[35] S. Talukdar, L. Emdad, S.K. Das, P.B. Fisher, EGFR: An essential receptor tyrosine kinase-regulator of cancer stem cells, in: 2020: pp. 161–188. https://doi.org/10.1016/bs.acr.2020.04.003.

[36] D.E. Heppner, M. Günther, F. Wittlinger, S.A. Laufer, M.J. Eck, Structural Basis for EGFR Mutant Inhibition by Trisubstituted Imidazole Inhibitors, J Med Chem 63 (2020) 4293–4305. https://doi.org/10.1021/acs.jmedchem.0c00200.

[37] J. O'Connell, J. Porter, B. Kroeplien, T. Norman, S. Rapecki, R. Davis, D. McMillan, T. Arakaki, A. Burgin, D. Fox III, T. Ceska, F. Lecomte, A. Maloney, A. Vugler, B. Carrington, B.P. Cossins, T. Bourne, A. Lawson, Small molecules that inhibit TNF signalling by stabilising an asymmetric form of the trimer, Nat Commun 10 (2019) 5795. https://doi.org/10.1038/s41467-019-13616-1.

[38] H. Wajant, K. Pfizenmaier, P. Scheurich, Tumor necrosis factor signaling, Cell Death Differ 10 (2003) 45–65. https://doi.org/10.1038/sj.cdd.4401189.

[39] J. Medler, H. Wajant, Tumor necrosis factor receptor-2 (TNFR2): an overview of an emerging drug target, Expert Opin Ther Targets 23 (2019) 295–307. https://doi.org/10.1080/14728222.2019.1586886.

[40] M.K. Kathiravan, A.B. Salake, A.S. Chothe, P.B. Dudhe, R.P. Watode, M.S. Mukta, S. Gadhwe, The biology and chemistry of antifungal agents: A review, Bioorg Med Chem 20 (2012) 5678–5698. https://doi.org/10.1016/j.bmc.2012.04.045.

[41] B. Zhai, X. Lin, Recent Progress on Antifungal Drug Development, Curr Pharm Biotechnol 12 (2011) 1255–1262. https://doi.org/10.2174/138920111796117292.

[42] X.-L. Wang, K. Wan, C.-H. Zhou, Synthesis of novel sulfanilamide-derived 1,2,3-triazoles and their evaluation for antibacterial and antifungal activities, Eur J Med Chem 45 (2010) 4631–4639. https://doi.org/10.1016/j.ejmech.2010.07.031.

[43] S.-L. Zhang, J.-J. Chang, G.L.V. Damu, B. Fang, X.-D. Zhou, R.-X. Geng, C.-H. Zhou, Novel berberine triazoles: Synthesis, antimicrobial evaluation and competitive interactions with metal ions to Human Serum Albumin, Bioorg Med Chem Lett 23 (2013) 1008–1012. https://doi.org/10.1016/j.bmcl.2012.12.036.

[44] T.M. Karpiński, Marine Macrolides with Antibacterial and/or Antifungal Activity, Mar Drugs 17 (2019) 241. https://doi.org/10.3390/md17040241.

[45] J. Munoz, J. Junior, F. Silva, Radziszewski Reaction: An Elegant, Easy, Simple and Efficient Method to Synthesise Imidazoles, Curr Org Synth 11 (2014) 824–834. https://doi.org/10.2174/1570179411666140623223611.

[46] N.M. Raghavendra, B.R.P. Kumar, P. Sasmal, G. Teli, R. Pal, P.M. Gurubasavaraja Swamy, B. Sajeev Kumar, Designing Studies in Pharmaceutical and Medicinal Chemistry, in: The Quintessence of Basic and Clinical Research and Scientific Publishing, Springer Nature Singapore, Singapore, 2023: pp. 125–148.

https://doi.org/10.1007/978-981-99-1284-1_9.

[47] O. Trott, A.J. Olson, AutoDock Vina: Improving the speed and accuracy of docking with a new scoring function, efficient optimization, and multithreading, J Comput Chem (2009) NA-NA. https://doi.org/10.1002/jcc.21334.

[48] H. Cheng, S.K. Nair, B.W. Murray, C. Almaden, S. Bailey, S. Baxi, D. Behenna, S. Cho-Schultz, D. Dalvie, D.M. Dinh, M.P. Edwards, J.L. Feng, R.A. Ferre, K.S. Gajiwala, M.D. Hemkens, A. Jackson-Fisher, M. Jalaie, T.O. Johnson, R.S. Kania, S. Kephart, J. Lafontaine, B. Lunney, K.K.-C. Liu, Z. Liu, J. Matthews, A. Nagata, S. Niessen, M.A. Ornelas, S.T.M. Orr, M. Pairish, S. Planken, S. Ren, D. Richter, K. Ryan, N. Sach, H. Shen, T. Smeal, J. Solowiej, S. Sutton, K. Tran, E. Tseng, W. Vernier, M. Walls, S. Wang, S.L. Weinrich, S. Xin, H. Xu, M.-J. Yin, M. Zientek, R. Zhou, J.C. Kath, Discovery of 1-{(3 R ,4 R)-3-[({5-Chloro-2-[(1-methyl-1 H -pyrazol-4-yl)amino]-7 H -pyrrolo[2,3- d]pyrimidin-4-yl}oxy)methyl]-4-methoxypyrrolidin-1-yl}prop-2-en-1-one (PF-06459988), a Potent, WT Sparing, Irreversible Inhibitor of T790M-Containing EGFR Mutants, J Med Chem 59 (2016) 2005–2024. https://doi.org/10.1021/acs.jmedchem.5b01633.

[49] G. Rimon, R.S. Sidhu, D.A. Lauver, J.Y. Lee, N.P. Sharma, C. Yuan, R.A. Frieler, R.C. Trievel, B.R. Lucchesi, W.L. Smith, Coxibs interfere with the action of aspirin by binding tightly to one monomer of cyclooxygenase-1, Proceedings of the National Academy of Sciences 107 (2010) 28–33. https://doi.org/10.1073/pnas.0909765106.

[50] J.L. Wang, D. Limburg, M.J. Graneto, J. Springer, J.R.B. Hamper, S. Liao, J.L. Pawlitz, R.G. Kurumbail, T. Maziasz, J.J. Talley, J.R. Kiefer, J. Carter, The novel benzopyran class of selective cyclooxygenase-2 inhibitors. Part 2: The second clinical candidate having a shorter and favorable human half-life, Bioorg Med Chem Lett 20 (2010) 7159–7163. https://doi.org/10.1016/j.bmcl.2010.07.054.

[51] M. Whitlow, A.J. Howard, D. Stewart, K.D. Hardman, L.F. Kuyper, D.P. Baccanari, M.E. Fling, R.L. Tansik, X-ray Crystallographic Studies of Candida albicans Dihydrofolate Reductase, Journal of Biological Chemistry 272 (1997) 30289–30298. https://doi.org/10.1074/jbc.272.48.30289.

[52] M. Gjorgjieva, T. Tomašič, M. Barančokova, S. Katsamakas, J. Ilaš, P. Tammela, L. Peterlin Mašič, D. Kikelj, Discovery of Benzothiazole Scaffold-Based DNA Gyrase B Inhibitors, J Med Chem 59 (2016) 8941–8954. https://doi.org/10.1021/acs.jmedchem.6b00864.

[53] J. O'Connell, J. Porter, B. Kroeplien, T. Norman, S. Rapecki, R. Davis, D. McMillan, T. Arakaki, A. Burgin, D. Fox III, T. Ceska, F. Lecomte, A. Maloney, A. Vugler, B. Carrington, B.P. Cossins, T. Bourne, A. Lawson, Small molecules that inhibit TNF signalling by stabilising an asymmetric form of the trimer, Nat Commun 10 (2019) 5795. https://doi.org/10.1038/s41467-019-13616-1.

[54] H.M. Berman, The Protein Data Bank, Nucleic Acids Res 28 (2000) 235–242. https://doi.org/10.1093/nar/28.1.235.

[55] BIOVIA, Discovery studio visualizer, (2020).

[56] M.U. Johansson, V. Zoete, O. Michielin, N. Guex, Defining and searching for structural motifs using DeepView/Swiss-PdbViewer, BMC Bioinformatics 13 (2012) 173. https://doi.org/10.1186/1471-2105-13-173.

[57] G.M. Morris, R. Huey, W. Lindstrom, M.F. Sanner, R.K. Belew, D.S. Goodsell, A.J. Olson, AutoDock4 and AutoDockTools4: Automated docking with selective receptor flexibility, J Comput Chem 30 (2009) 2785–2791. https://doi.org/10.1002/jcc.21256.

[58] A.W. Schüttelkopf, D.M.F. van Aalten, PRODRG : a tool for high-throughput crystallography of protein–ligand complexes, Acta Crystallogr D Biol Crystallogr 60 (2004) 1355–1363. https://doi.org/10.1107/S0907444904011679.

[59] B.N. Ostendorf, P. le Coutre, T.D. Kim, A. Quintás-Cardama, Nilotinib, in: 2014: pp. 67–80. https://doi.org/10.1007/978-3-642-54490-3_3.

[60] S.-H. Yoon, D.-Y. Cho, S. Choi, J. Lee, D.-K. Choi, E. Kim, J.-Y. Park, Synthesis and Biological Evaluation of Salicylic Acid Analogues of Celecoxib as a New Class of

Selective Cyclooxygenase-1 Inhibitor, Biol Pharm Bull 44 (2021) b20-00991. https://doi.org/10.1248/bpb.b20-00991.

[61] G. Piérard, J. Arrese, C. Piérard-Franchimont, Itraconazole, Expert Opin Pharmacother 1 (2000) 287–304. https://doi.org/10.1517/14656566.1.2.287.

[62] C.D. Freeman, N.E. Klutman, K.C. Lamp, Metronidazole, Drugs 54 (1997) 679–708. https://doi.org/10.2165/00003495-199754050-00003.

[63] C.A. Lipinski, F. Lombardo, B.W. Dominy, P.J. Feeney, Experimental and computational approaches to estimate solubility and permeability in drug discovery and development settings 1PII of original article: S0169-409X(96)00423-1. The article was originally published in Advanced Drug Delivery Reviews 23 (1997) 3–25. 1, Adv Drug Deliv Rev 46 (2001) 3–26. https://doi.org/10.1016/S0169-409X(00)00129-0.

[64] D.F. Veber, S.R. Johnson, H.-Y. Cheng, B.R. Smith, K.W. Ward, K.D. Kopple, Molecular Properties That Influence the Oral Bioavailability of Drug Candidates, J Med Chem 45 (2002) 2615–2623. https://doi.org/10.1021/jm020017n.

[65] A. Daina, O. Michielin, V. Zoete, SwissADME: a free web tool to evaluate pharmacokinetics, drug-likeness and medicinal chemistry friendliness of small molecules, Sci Rep 7 (2017) 42717. https://doi.org/10.1038/srep42717.

[66] A. Daina, V. Zoete, A BOILED-Egg To Predict Gastrointestinal Absorption and Brain Penetration of Small Molecules, ChemMedChem 11 (2016) 1117–1121. https://doi.org/10.1002/cmdc.201600182.

[67] P. Banerjee, A.O. Eckert, A.K. Schrey, R. Preissner, ProTox-II: a webserver for the prediction of toxicity of chemicals, Nucleic Acids Res 46 (2018) W257–W263. https://doi.org/10.1093/nar/gky318.

[68] D. Gfeller, A. Grosdidier, M. Wirth, A. Daina, O. Michielin, V. Zoete, SwissTargetPrediction: a web server for target prediction of bioactive small molecules, Nucleic Acids Res 42 (2014) W32–W38. https://doi.org/10.1093/nar/gku293.

[69] M.J. Abraham, T. Murtola, R. Schulz, S. Páll, J.C. Smith, B. Hess, E. Lindahl, GROMACS: High performance molecular simulations through multi-level parallelism from laptops to supercomputers, SoftwareX 1–2 (2015) 19–25. https://doi.org/10.1016/j.softx.2015.06.001.

[70] D.M. van Aalten, A. Amadei, R. Bywater, J.B. Findlay, H.J. Berendsen, C. Sander, P.F. Stouten, A comparison of structural and dynamic properties of different simulation methods applied to SH3, Biophys J 70 (1996) 684–692. https://doi.org/10.1016/S0006-3495(96)79608-X.

[71] D. Schneidman-Duhovny, O. Dror, Y. Inbar, R. Nussinov, H.J. Wolfson, PharmaGist: a webserver for ligand-based pharmacophore detection, Nucleic Acids Res 36 (2008) W223–W228. https://doi.org/10.1093/nar/gkn187.